



# LUND UNIVERSITY

## An mTRAN-mRNA interaction mediates mitochondrial translation initiation in plants

Tran, Huy Cuong; Schmitt, Vivian; Lama, Sbatie; Wang, Chuande; Launay-Avon, Alexandra; Bernfur, Katja; Sultan, Kristin; Khan, Kasim; Brunaud, Veronique; Liehrmann, Arnaud; Castandet, Benoit; Levander, Fredrik; Rasmusson, Allan; Mireau, Hakim; Delannoy, Etienne; Van Aken, Olivier

*Published in:*  
Science

2023

*Document Version:*  
Peer reviewed version (aka post-print)

[Link to publication](#)

*Citation for published version (APA):*

Tran, H. C., Schmitt, V., Lama, S., Wang, C., Launay-Avon, A., Bernfur, K., Sultan, K., Khan, K., Brunaud, V., Liehrmann, A., Castandet, B., Levander, F., Rasmusson, A., Mireau, H., Delannoy, E., & Van Aken, O. (2023). An mTRAN-mRNA interaction mediates mitochondrial translation initiation in plants. *Science*, 381(6661), Article adg0995. <https://www.science.org/doi/10.1126/science.adg0995>

*Total number of authors:*  
16

*Creative Commons License:*  
CC BY

### General rights

Unless other specific re-use rights are stated the following general rights apply:  
Copyright and moral rights for the publications made accessible in the public portal are retained by the authors and/or other copyright owners and it is a condition of accessing publications that users recognise and abide by the legal requirements associated with these rights.

- Users may download and print one copy of any publication from the public portal for the purpose of private study or research.
- You may not further distribute the material or use it for any profit-making activity or commercial gain
- You may freely distribute the URL identifying the publication in the public portal

Read more about Creative commons licenses: <https://creativecommons.org/licenses/>

### Take down policy

If you believe that this document breaches copyright please contact us providing details, and we will remove access to the work immediately and investigate your claim.

LUND UNIVERSITY

PO Box 117  
221 00 Lund  
+46 46-222 00 00

# **An mTRAN-mRNA interaction mediates mitochondrial translation initiation in plants**

Huy Cuong Tran<sup>1</sup>, Vivian Schmitt<sup>1</sup>, Sbatie Lama<sup>1,2</sup>, Chuande Wang<sup>3</sup>, Alexandra Launay-Avon<sup>4,5</sup>, Katja Bernfur<sup>6</sup>, Kristin Sultan<sup>7</sup>, Kasim Khan<sup>1</sup>, Véronique Brunaud<sup>4,5</sup>, Arnaud Liehrmann<sup>4,5,8</sup>, Benoit Castandet<sup>4,5</sup>, Fredrik Levander<sup>7,9</sup>, Allan G. Rasmusson<sup>1</sup>, Hakim Mireau<sup>3</sup>, Etienne Delannoy<sup>4,5</sup>, Olivier Van Aken<sup>1\*</sup>

<sup>1</sup> Department of Biology, Lund University, Lund, Sweden

<sup>2</sup> Current address: Department of Plant Breeding, Swedish University of Agricultural Sciences, Alnarp, Sweden

<sup>3</sup> Université Paris-Saclay, INRAE, AgroParisTech, Institut Jean-Pierre Bourgin (IJPB), 78000, Versailles, France

<sup>4</sup> Université Paris-Saclay, CNRS, INRAE, Université d'Évry, Institute of Plant Sciences Paris-Saclay (IPS2), 91405, Orsay, France

<sup>5</sup> Université Paris Cité, CNRS, INRAE, Institute of Plant Sciences Paris-Saclay (IPS2), 91405, Orsay, France

<sup>6</sup> Department of Chemistry, Lund University, Lund, Sweden

<sup>7</sup> Department of Immunotechnology, Lund University, Lund, Sweden

<sup>8</sup> Université Paris-Saclay, CNRS, Université d'Évry, Laboratoire de Mathématiques et Modélisation d'Évry, 91037, Évry-Courcouronnes, France

<sup>9</sup> National Bioinformatics Infrastructure Sweden, Science for Life Laboratory, Lund University, Lund, Sweden

\*Corresponding author      Olivier Van Aken  
Molecular Cell Biology Unit  
Department of Biology  
Lund University  
Sölvegatan 35  
Lund 223 62 – Lund, Sweden  
Tel: +46 76 210 14 03  
E-mail: [olivier.van\\_aken@biol.lu.se](mailto:olivier.van_aken@biol.lu.se)

## **ABSTRACT**

Plant mitochondria represent the largest group of respiring organelles on our planet. Plant mitochondrial mRNAs lack Shine-Dalgarno-like ribosome-binding sites, so it is unknown how plant mitoribosomes recognize mRNA. We show that “mitochondrial translation factors” mTRAN1/mTRAN2 are land plant-specific proteins, required for normal mitochondrial respiration chain biogenesis. Our studies suggest mTRANs are non-canonical pentatricopeptide repeat (PPR)-like RNA-binding proteins of the mitoribosomal “small” subunit. We identified conserved A/U-rich motifs in the 5’ regions of plant mitochondrial mRNAs. mTRAN1 binds this motif, suggesting it is a mitoribosome homing factor to identify mRNAs. We demonstrate that mTRANs are likely required for translation of all plant mitochondrial mRNAs. Plant mitochondrial translation initiation thus appears to use a protein-mRNA interaction that is divergent from bacteria or mammalian mitochondria.

Although most mitochondrial proteins are nuclear-encoded, mitochondria have partially retained their genome and translational machinery (1, 2). In plants, the number of unique mitochondrial proteins is estimated around 1000 to >2000 (2, 3), but the mitochondrial genome only encodes 20–40 proteins (4, 5). Despite a bacterial origin, mitochondrial translation is substantially different from its bacterial counterpart (6-8). In yeast, mitochondrial translation initiation is regulated by general translational factors associated with the mitoribosome and mRNA-specific factors that bind 5'-untranslated regions (5' UTRs) to position translation initiation sites (9, 10). Mammalian mitochondrial mRNAs have absent or extremely short 5' UTRs and translation can start directly on non-AUG start codons (11, 12).

Bacterial-type Shine–Dalgarno ribosome-binding sequences are not found in flowering plant mitochondrial 5' UTRs (13). Therefore, there is poor understanding of how plant mitoribosomes interact with 5' UTRs of mitochondrial mRNAs and how mitoribosomal small subunits (mtSSU) identify correct translation start codons. In contrast with other species, the plant mtSSU is larger than the mitoribosomal large subunit (mtLSU) (14, 15). The plant mitoribosome structure and core components have recently been studied (14-16), showing plant-specific ribosomal pentatricopeptide repeat (rPPR) proteins have become bona fide ribosomal constituents. PPR proteins contain repeats of 35 amino-acid tandem motifs, each forming two anti-parallel  $\alpha$ -helices, which interact with each other to generate a helix-turn-helix motif (17, 18). The helix-turn-helix PPR domains form a superhelix with a central groove, allowing PPR proteins to interact with RNA (17, 19).

Here, we characterized Arabidopsis genes *AT4G15640* and *AT3G21465*, currently annotated as adenylyl cyclases (ACs), but also suggested to be mitochondrial ribosome components *rPPR10/mS83* (*ribosomal pentatricopeptide repeat protein 10*) (14, 15). ACs catalyze conversion of ATP to 3'-5'-cyclic adenosine monophosphate (cAMP) – a second messenger that affects different physiological and biochemical processes. ACs have been extensively studied in animals, but little is known about ACs in plants (20, 21). As our results indicate that *AT4G15640* and *AT3G21465* are not classical PPR proteins, but required for translation initiation by plant mitoribosomes, we propose a new annotation for *AT4G15640* and *AT3G21465*: MITOCHONDRIAL TRANSLATION FACTOR 1 (mTRAN1) and mTRAN2, respectively.

### **mTRAN1 and mTRAN2 are plant-specific proteins**

Using a BLAST search, we found that mTRAN1 (AT4G15640) and mTRAN2 (AT3G21465) are present only in *Embryophyta* (land plants). Protein sequence alignment showed that mTRAN1/2 are highly similar (84% identical), suggesting they are paralogs in *Arabidopsis thaliana*. Some angiosperms, including *Brassicaceae* and *Glycine max* contain two mTRAN proteins (Fig. 1A and S1), indicating that the duplication event of mTRAN protein-encoding genes occurred relatively late in evolution, with the divergence of *Fabaceae* dating back around 70 million years (22). *Physcomitrium patens*, a non-vascular moss, also has two mTRAN proteins, suggesting independent duplication events have occurred (23). The remaining land plant species examined here contain only one mTRAN protein.

### **mTRAN1 and mTRAN2 are targeted to mitochondria**

Prediction analyses suggested that mTRAN1 is mitochondrially targeted (24) and this was supported by mitochondrial complexome profiling (25). To confirm mTRAN mitochondrial localization, we stably expressed mTRAN1-GFP and mTRAN2-GFP fusions in *Arabidopsis* Col-0 plants. mTRAN1-GFP and mTRAN2-GFP co-localized with the MitoTracker fluorescent dye that labels mitochondria (Fig. 1B). Additionally, we performed immunoblot analysis on purified cytosolic, mitochondrial and chloroplastic fractions isolated from *Arabidopsis* seedlings expressing mTRAN1/2-GFP (Fig. 1C). mTRAN1-GFP and mTRAN2-GFP could only be detected in the mitochondrial fractions, further confirming their mitochondrial location.

### **The *mtran* mutants have a growth reduction phenotype**

*mTRAN1* and *mTRAN2* genes show relatively similar expression patterns during plant development (Fig. S2). Of note, mTRAN proteins are expressed very early in seeds during germination (one day after imbibition) (Fig. S2), suggesting they might be critical for plant development. Three independent knockout lines were obtained for each *mTRAN* gene (Fig. S3A). We obtained double homozygous knockout plants for *mtran1-1* x *mtran2-1* (*mtran1-1/2-1*) and *mtran1-2* x *mtran2-2* (*mtran1-2/2-2*), and verified loss of *mTRAN1* and *mTRAN2* transcripts by qRT-PCR (Fig. S3D). Only plants homozygous for either *mtran1-3* or *mtran2-3*, and hemizygous for the other mutations, could be obtained, indicating that *mtran1-3/2-3* was non-viable (Fig. S3B and S3C). The *mtran1* single mutants were smaller than Col-0 wild type (WT), while the *mtran2* mutants appeared more similar in size to WT (Fig. 1D). *mtran1-1/2-1* was also smaller than WT, while *mtran1-2/2-2* showed severe growth retardation. *mtran* single and double mutants were significantly slower to germinate (stage 0.5) and develop true leaves

(stage 1.02/1.04) (Fig. 1E) (26). Primary roots of the *mtran* single and double mutants were significantly shorter than those of the wild type (WT) (Fig. S3E). Again, the double mutants showed a >80% reduction in primary root growth. Additionally, *mtran* single and double mutants were significantly smaller and slower to flower than WT (Fig. S3F). *Mtran1-2/2-2* had a stronger phenotype compared to *mtran1-1/2-1* (Fig. 1D-F). The milder phenotype of *mtran1-1/2-1* is likely because of the presence of the T-DNA in the 10<sup>th</sup> intron of *mTRAN1*, potentially resulting in a partially active protein. For *mTRAN1*, the T-DNA is inserted in the 5<sup>th</sup> and 7<sup>th</sup> exon likely resulting in severe growth deficiency and lethality of *mtran1-2/2-2* and *mtran1-3/2-3*, respectively.

### **mTRAN1 and mTRAN2 are unlikely to be adenylyl cyclases**

mTRAN1 and mTRAN2 are annotated as ACs, but we could not find experimental evidence nor a defined source for this annotation. To evaluate mTRAN1/2 AC activity, we performed a bacterial cAMP synthase complementation assay in the *BTH101 (cya)* *E. coli* strain that lacks endogenous AC activity (27). The cells transformed with the positive control formed colored colonies on MacConkey/maltose and LB/X-gal media, and could grow on M63 medium (Fig. S4A). *mTRAN1* and *mTRAN2* were cloned into the pUT18 vector and transformed into *E. coli cya*. On all tested media, pUT18-*mTRAN1* and pUT18-*mTRAN2* colonies had the same phenotype as the negative pUT18 control (Fig. S4A). Thus, *mTRAN1* and *mTRAN2* do not appear to have AC activity in the bacterial system, though we cannot rule out a false negative result as *E. coli* may not provide the correct environment for plant ACs. Furthermore, there was no significant difference in cAMP concentration between the WT and the *mtran* double knockout mutants (Fig. S4B), despite their clear growth retardation phenotype (Fig. 1D-F), supporting the idea that mTRAN1 and mTRAN2 are unlikely to be ACs.

### **Mitochondrial oxidative phosphorylation complexes show reduced activity in *mtran* double mutants**

To find the cause for slow growth of *mtran* double mutants, mitochondria isolated from *mtran1-1/2-1* and *mtran1-2/2-2* were analyzed by Blue Native-Polyacrylamide gel electrophoresis (BN-PAGE). The *mtran* double mutants showed a decrease in abundance of supercomplex I/III, complex I, III and V compared to WT (Fig. 2A-B). Furthermore, the activity of complex I, III, IV and V was reduced in the *mtran* double mutants, especially *mtran1-2/2-2* (Fig. 2C). Freshly isolated mitochondria from *mtran1-1/2-1* and *mtran1-2/2-2* were used for oxygen consumption measurements (Fig. 2D). The state III respiration rates

(succinate+ADP+NADH) of *mtran* double mutants were significantly lower compared to WT. The *mtran* double mutants however had a significantly higher alternative oxidase (AOX) pathway capacity (KCN+DTT+pyruvate). Additionally, the ratio of AOX capacity to state III was significantly higher in the *mtran* double mutants, suggesting they rely heavily on alternative respiration.

### **Loss of *mTRAN1* and *mTRAN2* causes changes in abundance of mitochondrial proteins**

In the *mtran* double mutants, especially *mtran1-2/2-2*, proteins from complex I, III, IV and V were less abundant (Fig. 2E), in agreement with the decrease in abundance and activity of these complexes (Fig. 2A-C). Mitochondrially-encoded mitoribosomal subunits RIBOSOMAL PROTEIN S4 (RPS4) and RIBOSOMAL PROTEIN L16 (RPL16), and nuclear-encoded mitochondrial translation factor LEUCINE ZIPPER-EF-HAND-CONTAINING TRANSMEMBRANE PROTEIN 1 (LETM1) were more abundant in the *mtran* double mutants. Nuclear-encoded mtSSU subunit RIBOSOMAL PROTEIN S10 (RPS10) did not show clear differences in abundance in the mutants.

Proteins encoded by mitochondrial retrograde signaling marker genes, including ALTERNATIVE OXIDASE (AOX), UP REGULATED BY OXIDATIVE STRESS (UPOX) and TRANSLOCASE OF THE INNER MEMBRANE 17 (TIM17) (28, 29), were more abundant in both double mutants. This indicates that loss of *mTRAN1* and *mTRAN2* induced mitochondrial retrograde/ unfolded protein response (UPR<sup>mt</sup>) signaling (Fig. 2E). Upregulation of AOX protein is consistent with the reliance of *mtran* double mutants on alternative respiration (Fig. 2C).

To assess global changes in mitochondrial protein abundance, we analyzed isolated mitochondria with tandem mass spectrometry (MS/MS) (Data S1). We detected mTRAN1 in WT and *mtran1-1/2-1* mitochondria, with comparable abundance. However, mTRAN1 was not detected in *mtran1-2/2-2*. This is consistent with our hypothesis regarding mTRAN1 activity and the location of the T-DNA insertion in *mTRAN1*. mTRAN2 could not be detected in any of the genotypes, suggesting mTRAN1 is much more abundant than mTRAN2, in agreement with a recent study (3). This may explain why we found 684 and 24 proteins to be significantly different in abundance in *mtran1-2/2-2* and *mtran1-1/2-1* ( $P_{\text{adj}} < 0.2$ ), respectively, compared to WT. Using a less stringent unadjusted  $P < 0.05$ , 247 proteins were found to be differentially abundant in the *mtran1-1/2-1* mitochondria, representing subunits of complex I, III, IV and V, in agreement with immunoblot results (Fig. 2E). Of the 684 proteins affected in *mtran1-2/2-2*,

mitochondrially-encoded oxidative phosphorylation (OXPHOS) proteins, including NADH DEHYDROGENASE 1, 7 and 9 (Nad1, Nad7 and Nad9), APOCYTOCHROME B (Cob), CYTOCHROME OXIDASE 2 (Cox2), and ATP SYNTHASE SUBUNIT 1, 4 and 8 (Atp1, Atp4 and Atp8), were less abundant. However, subunits of complex II, all of which are nuclear-encoded, were not affected in the mutants. Mitochondrially-encoded RIBOSOMAL PROTEIN L5 (Rpl5) and Rpl16, and nuclear-encoded AOX1A, AOX1D and LETM1 were more abundant. This is consistent with the results of our immunoblot analysis. Furthermore, heat shock proteins, ADP/ATP carrier proteins, ALTERNATIVE NAD(P)H DEHYDROGENASES NDA1/NDB2, proteases, mitochondrially-targeted ribosomal proteins, PPR/MORF proteins, ovule abortion (OVA) proteins, and amino acid-tRNA ligases were more abundant. In conclusion, loss of both mTRAN proteins results in severe perturbation of the mitochondrial proteome and reduction of many OXPHOS components.

### **mTRAN1 and mTRAN2 are part of the mitoribosome small subunit**

To identify mTRAN1/2-interacting proteins, plants expressing mTRAN1-GFP or mTRAN2-GFP were used for co-immunoprecipitation (co-IP) followed by MS/MS. A mitochondria-targeted GFP line (mito-GFP) (30) was used as negative control. The phenotypes of complementation lines *mtran1-2/2-2 35S:mTRAN1-GFP* and *mtran1-2/2-2 35S:mTRAN2-GFP* were similar to WT (Fig. S5), indicating that mTRAN1-GFP and mTRAN2-GFP proteins are fully functional. A summary of proteins co-immunoprecipitated with mTRAN1-GFP and mTRAN2-GFP is presented in Data S2A. We found that mTRAN1 and mTRAN2 interacted with 27 components of the mtSSU, as proposed by previous work (14, 15). In contrast, no mitoribosome core subunits were pulled down using the mito-GFP control, indicating the specificity of the interactions. This indicates that mTRAN1 and mTRAN2 are part of the mtSSU. All ribosomal proteins interacting with mTRAN proteins belonged to the mtSSU, except mitochondrial ribosomal protein L11, which is part of the mtLSU. mtLSU L11 was however only identified in the first replicate. Most rPPR proteins found in Waltz et al (15) and Rugen et al (14) interacted with mTRAN proteins, though rPPR3a (AT1G55890) only co-immunoprecipitated with mTRAN1. An individual mitochondrion contains on average around 520 copies of mtSSU proteins (3), which is very close to the estimated 534 copies found for mTRAN1, supporting the idea that mTRANs are integral parts of the plant mitoribosome. We also found proteins interacting with mTRAN proteins that were only detected in our analysis (Data S2A, gray color), including three additional mitochondrially-targeted ribosomal proteins, a PPR protein (AT3G61520) and MORF8. mTRAN1 and mTRAN2 also interacted with

mitochondrially-encoded Nad7 and Nad9, which are less abundant in the *mtran* double mutants (Fig. 2, Data S1). Overall, our co-IP results demonstrate that mTRAN1/2 are part of the mtSSU, suggesting they might be involved in mitochondrial translation.

### **Transcriptome analysis of *mtran1-2/2-2* indicates mitochondrial translation defects**

RNA-seq analysis was carried out on WT and *mtran1-2/2-2*, (Fig. 1D-F). 2143 nuclear-encoded differentially expressed genes (DEGs;  $P_{\text{adj}} < 0.05$ , fold change  $> 2$  or  $< 0.5$ ) were found in *mtran1-2/2-2* versus WT, of which 1117 were upregulated and 1026 were downregulated (Data S3). Gene ontology analysis showed that stress-responsive genes were upregulated, while oxygen level, hypoxia and hormone (auxin) responsive genes were downregulated (Data S4). Mitochondrial retrograde signaling marker genes such as *AOX1a* were significantly upregulated (Data S3), indicating that loss of *mTRAN1* and *mTRAN2* activates UPR<sup>mt</sup> signaling likely via ANAC017 (31). We confirmed upregulation of UPR<sup>mt</sup> marker genes in *mtran1-2/2-2* and *mtran1-1/2-1* by qRT-PCR (Fig. S6A).

Next, the RNA-seq dataset of *mtran1-2/2-2* was compared with the transcript profiles of 22 additional Arabidopsis mutants and chemical treatments affecting mitochondrial function (Fig. 3A, Data S5A). The similarities among all datasets were evaluated by comparison of common pairwise DEGs calculated via the Sørensen-Dice similarity coefficient (DSC) (Data S5B), followed by hierarchical clustering of the complete DSC matrix (Fig. 3A). *mtran1-2/2-2* clustered most closely with the *rps10* P2 and P3 mutants, in which transcript levels of mtSSU-subunit *RPS10* are reduced (32). This further supports that mTRANs are involved in mitochondrial translation. *mtran1-2/2-2* also clustered relatively closely to antimycin A (AA) (inhibitor of complex III), oligomycin (inhibitor of complex V) and rotenone (inhibitor of complex I) datasets, in line with the observed loss of activity of these complexes in *mtran* double mutants (Fig. 2). We then visualized the similarities of nuclear transcript profiles among *mtran1-2/2-2*, *rps10* mutants and prohibitin *atphb3* mutant (29), which did not cluster closely to *mtran1-2/2-2* (Fig. S6B). *mtran1-2/2-2* shared 326 and 651 DEGs with *rps10* P2 and P3, respectively, whereas 106 common DEGs were found between *mtran1-2/2-2* and *atphb3*. 288 DEGs were commonly found between *mtran1-2/2-2* and both *rps10* mutants. 31 DEGs were common among all genotypes, including many UPR<sup>mt</sup> markers like *AOX1a* (Fig. S6C).

We also analyzed *mtran1-2/2-2* mitochondrial and chloroplast transcript profiles (Data S6). All 57 mitochondrially-encoded genes were significantly upregulated ( $\text{FC} > 1.4$ ,  $P_{\text{adj}} < 0.05$ ), ranging in fold change up to 4.39x for *trnY* (Data S6A). Mitochondrial transcription thus seems globally

increased, which may be a compensation response to reduced translation. All 6 genes that were more than 4x induced encoded tRNAs, further suggesting an attempt to compensate for reduced translation. The mitochondrial transcriptome was further compared to mitochondrial/chloroplast RNA polymerase *rpotmp* and *atphb3* mutants (29, 33). While in *rpotmp* and *atphb3* mutants a mix of up- and down-regulated genes could be observed, in *mtran1-2/2-2* nearly all genes were upregulated (Fig. S6D, Data S6C). In contrast, all 117 annotated chloroplast-encoded genes were slightly downregulated ( $P_{\text{adj}} < 0.05$ ) (Data S6B). In conclusion, loss of mTRAN1/2 resulted in increased expression of nearly all mitochondrially-encoded genes, suggesting that the cells attempted to compensate for reduced mitochondrial translation.

Next, we analyzed the mitochondrial transcriptome for alterations in splicing and editing (Data S7). The rate of C-to-U editing was significantly different between *mtran1-2/2-2* and WT for 262 cytosines ( $\text{FDR} < 0.05$ ) (Data S7A). The majority (208) of these editing sites were relatively less edited in the mutant than in WT (Data S7A). However, considering that mitochondrial transcripts were more abundant in *mtran1-2/2-2*, for 244 differentially edited sites there were still more edited transcripts in absolute terms in *mtran1-2/2-2* compared to in WT. We therefore suggest that there are more than enough correctly-edited mitochondrial transcripts in *mtran1-2/2-2* mitochondria to allow production of the correct proteins. For six mitochondrial transcript splice sites, a significant difference was observed in the mutants versus WT ( $\text{FDR} < 0.05$ ) (Data S7B). Also here, for all transcripts there was a higher absolute number of spliced transcripts in the mutant, indicating that the lower abundance of many mitochondrially-encoded proteins (Fig. 2) is not caused by a lack of correctly spliced/edited mitochondrial transcripts. The observed similarities in nuclear transcriptome between *mtran1-2/2-2* and *rps10* mutants, and excessive expression of mitochondrial transcripts, thus point to a defect in mitochondrial translation.

### **mTRAN1 and mTRAN2 are required for translation in mitochondria**

To validate whether mitochondrial translation was indeed affected in the *mtran* double mutants, we performed in organello protein synthesis assays using freshly isolated mitochondria from Arabidopsis seedlings. Synthesized radiolabelled mitochondrial translation products were evaluated after 10, 30 and 60 min of translation (Fig. 3B and S7). Sodium acetate, a unique substrate for bacterial translation, was used to evaluate bacterial contamination during mitochondrial purification. We could identify several distinct protein bands, including Atp1,

Cob, Cox2 and Atp9, based on their molecular mass (34, 35). Atp1, Cob, Cox2 and Atp9 had a slower rate of translation in the *mtran* double knockout mutants than in the WT. This was consistent with our immunoblot and MS/MS analysis (Fig. 2E, Data S1), in which we observed a reduction in the abundance of Atp1 and Cox2 in the *mtran* double knockout mutants. Thus, mTRAN1 and mTRAN2 are required for efficient translation in mitochondria.

The efficiency of translation depends on both translation initiation and elongation. If translation initiation is impaired, one would expect fewer ribosomes attached to a given mRNA. If translation elongation is defective, one would expect more ribosomes attached to the mRNA, due to difficulties in completing translation. To allow us to distinguish between these two possibilities in the *mtran* double mutants, we assessed ribosome-loading along mitochondrially-encoded transcripts in mutants and WT (Fig. 3C). Polysomes are composed of mRNAs bound to two or more ribosomes, whereas monosomes consist of mRNAs bound to a single ribosome and/or “vacant couples”, which are stable associations of small and large ribosomal subunits without binding mRNAs (36). In this analysis, polysomes were separated from monosomes and free mRNAs by sucrose gradient ultracentrifugation. After centrifugation, we collected 10 fractions along the gradient (fraction 1-10 from light to heavy), and performed qRT-PCR to determine the percentage of mitochondrial mRNA present in each fraction (Fig. 3C). Overall, all analyzed mitochondrially-encoded mRNAs of both *mtran1-1/2-1* and *mtran1-2/2-2* distributed mainly in fractions 2 and 3, whereas mRNAs in WT were mostly found in fractions 3 and 4 (Fig. 3C). These shifts towards the lighter fractions indicate that the number of ribosomes associated with the mRNAs was lower in the *mtran* double mutants, suggesting inefficient translation initiation/mitoribosomal binding to mRNAs. To determine the distribution of the mitoribosomes, we analyzed 18S rRNA (*rrn18*) of mtSSU and 26S rRNA (*rrn26*) of mtLSU. The *rrn18* of the WT was mainly found in fraction 3 and 4, and *rrn26* was mainly in fraction 4, colocalizing with protein-encoding mRNAs (Fig. 3C). This indicates that most WT mRNAs are bound by mitoribosomes and are actively translated. In *mtran1-2/2-2*, *rrn18* was still present mainly in fraction 3 and 4, as observed in the WT. *rrn26* was however spread out over the lighter fractions 2-4, suggesting mtLSU is not efficiently translating in *mtran1-2/2-2*. In *mtran1-1/2-1*, the mitoribosomes were mainly found in the heavy fractions 8-9, and to a lesser extent in fractions 3 and 5, as opposed to in the lighter fractions 2-4 as observed in *mtran1-2/2-2*.

In all cases, the mRNA levels in fraction 2 were much higher in the mutants than in the WT. Because fraction 2 contains almost no mitoribosomes according to our analysis (Fig. 3C and

S8), our results indicate that a large proportion of mitochondrial mRNAs are likely devoid of ribosomes in the *mtran* double mutants. In *mtran1-1/2-1*, a small percentage of several mRNAs was found in fractions 8-9 indicating they are heavily translated by polysomes (see discussion). However, no obvious effect of loss of mTRANs could be detected on cytosolic translation, as assessed by ribosome-loading of nuclear-encoded *UBIQUITIN-CONJUGATING ENZYME 21* (*UBC21*). Together, our findings provide evidence that mTRAN proteins are key components of plant mitoribosomes required for translation initiation.

### **Structural modelling suggests that mTRAN proteins have PPR protein like-structures**

Because mTRAN proteins are part of the mtSSU (Data S2) and required for translation (Fig. 3), we assessed predicted protein structures to anticipate if the proteins could bind mitochondrial mRNAs to help mtSSU initiate translation. Structures of mTRAN proteins without the predicted mitochondrial targeting sequences (MTS) (37) were modelled using AlphaFold (38), RoseTTAFold (39) and iTASSER (40) (Fig. S9). The modelled partial mTRAN1 structure extracted from the cryo-EM structure of the mitoribosome from *Brassica oleracea* var. *botrytis* (cauliflower) (16) is also presented for comparison (Fig. S9). Overall, the protein structures shown by prediction tools and Waltz et al (16) suggest that mTRAN1 and mTRAN2 have tetratricopeptide-repeat (TPR)/PPR protein like-structures. PPR proteins are known as RNA-binding proteins involved in RNA processing, splicing, stability, editing, and translation (19, 41). The three programs predicted that mTRAN1 and mTRAN2 contain 8-10 PPR-like repeats. The cryo-EM structure of the plant mitoribosome by Waltz et al (16) proposed that mTRAN1 is formed by 6 PPR-like repeats, based on the number of PPR repeats predicted by 'TPRpred' software (42).

We then attempted to find potential mTRAN-RNA target sites using aPPRove (43) and the PPRCODE prediction server (44), but were unable to find potential RNA-binding sites for mTRAN1 and mTRAN2. This suggests mTRANs belong to a PPR-like protein class that does not obey the standard PPR code and may bind RNA differently.

### **mTRAN1 binds to putative mitoribosome binding sites in mitochondrial 5' UTRs**

As potential RNA binding sites could not be predicted for mTRANs using the PPR code, we searched for potential conserved mitoribosome binding sites in the 5' UTRs of mitochondrial mRNAs. Using the Multiple Expectation-maximization for Motif Enrichment (MEME) motif search tool, we identified a potential CUUUxU-like mitoribosome binding site in the 5' UTRs of 26 mitochondrial mRNAs (Fig. 4A and S10, Data S8B and S8C). Waltz et al (16) suggested

that the plant mitoribosome might recognize an AxAAA-related motif, which is located 19 bases upstream of the start codons in 17 mitochondrial mRNA 5' UTRs. The MEME motif search tool was unable to identify the AxAAA-related motif, but we found a similar AAGAAx-like motif in 30 5' UTRs when including the intercistronic UTRs (Fig. 4A and S10, Data S8C). Furthermore, we manually found an overlapping AxAAAG-like motif in the 5' UTRs of 17 mitochondrial mRNAs (Fig. 4A and S10, Data S8B and S8C). In summary, we identified at least one CUUUxU or AAGAAx/AxAAAG motif in the 5' regions of all 30 mitochondrial mRNAs (Fig. S10).

Next, we searched the 5' upstream genomic regions for hexamers enriched at any given position in 49706 mitochondrially-encoded genes of seed plants, 4256 of mosses, 2659 of liverworts and 7867 of green algae, using "PLMdetect" (45, 46) (Fig. S11). In seed plants, there is a preference for enriched motifs around position -25 upstream of the start codon, but the location of the motifs is more variable, extending beyond 100 bases upstream and into the coding sequence. Similar diffuse preferences were observed in mosses and liverworts, with peaks situated around -25/-28 or -27, respectively. Analysis of 7867 green algae mitochondrial gene 5' genomic regions revealed an extremely tight peak at -25, and nearly no signal elsewhere (Fig. S11). The sequences of the motifs enriched around -25 in seed plants were A-rich and related to AAGAAA/AGAAAA, similar to those we defined in Arabidopsis (Fig. S11, Data S9). Over half of the tested seed plant 5' regions had such a motif around the -25 position. Also in mosses and liverworts AAAAAA/AAAAAG-like motifs were present in the majority of 5' UTRs around -25/-28 or -27, respectively. In green algae almost complete conservation of strictly A/U containing hexamers was found around -25 of the start codon (Fig. S11, Data S9). Being based on genomic data, the presence of these motifs in mature mRNAs requires further validation. The CUUUxU motif was found in all lineages in 3-4% of the genes with a different preferential position: -28 in seed plants and -69 in green algae. Overall, A/U-rich motifs appear to be a common feature in most 5' sequences of plant mitochondrial mRNAs, suggesting they may serve as ribosome binding sites.

As mTRAN1 is the main isoform in Arabidopsis, we performed RNA electrophoretic mobility shift assays (REMSAs) to test whether mTRAN1 can bind to the CUUUxU or AAGAAx/AxAAAG motifs identified in 5' UTRs of mitochondrial mRNAs (Fig. 4 and S12). Synthesized Cy5-labelled RNA probes, containing one or more of the predicted mitoribosome binding motifs in the 5' UTRs of *nad9*, *nad7*, *cox2*, *cox3* and *rpl5/cob* were obtained (Fig. 4A-B). Mutated probes were also synthesized to verify the specificity of mTRAN1 binding. The

REMSAs showed that mTRAN1 could bind the WT *nad9*, *nad7*, *cox2*, *rpl5/cob* and *cox3* probes specifically, while the interactions were lost when the predicted CUUUxU/AAGAAx/AxAAAG motifs were specifically mutated (Fig. 4C). Although a weak shift was observed in the *nad7* mutated probe, it was clear that mTRAN1 bound more strongly (lower  $K_d$ ) to the WT than mutated probe (Fig. 4C, Fig. S12C-D). The binding of mTRAN1 appeared stronger (lower  $K_d$ ) to AAGAAx/AxAAAG motifs than to CUUUxU motifs (Fig. S12C-D).

To establish whether mTRAN1 binds the 5' UTRs of mitochondrial mRNAs in vivo, we performed RNA immunoprecipitation sequencing (RIP-seq) on isolated mitochondria from the *mTRAN1-GFP* lines, using *mito-GFP* as a control. To discriminate the mTRAN1-specific immunoprecipitated RNA fragments from the GFP-control background, we used “DiffSegR” (48, 49), which delineates boundaries of differential regions without using pre-existing annotations, allowing precise identification of enriched regions. The RIP-seq analysis showed that mTRAN1 binds 5' UTR regions, generally preferring the UTRs to CDS (Fig. 5A). Furthermore, we observed clear evidence that the mTRAN1-bound 5' UTR regions contained the same CUUUxU/AAGAAx/AxAAAG motifs for *nad9*, *cox2* and *cox3* as used for the REMSAs (Fig. 4 and 5B). The *rps4* mRNA has no 5' UTR, but we found an mTRAN1-interacting segment at the 5' of the mRNA, with a clear peak covering an AAAAAA motif positioned 13 bases after the ATG (Fig. 5B). Significant mTRAN1-bound regions were found in the 5' UTR or just downstream of the AUG for 17 protein-encoding genes. A MEME motif search of these regions confirmed enrichment of CUUUxU and AAGAAx motifs (Data S10). Together, our findings indicate that mTRAN1 binds to CUUUxU and AAGAAx/AxAAAG-like motifs, which are potential mitoribosome binding sites in the 5' regions of plant mitochondrial mRNAs, to initiate translation.

### **mTRAN proteins are likely universal plant mtSSU translation initiation factors**

To further assess how translation of mitochondrial mRNAs is affected in the *mtran* mutants, we performed ribosome profiling analysis (Ribo-seq), in which short RNase-protected mRNA fragments covered by the translating ribosomes (called ribosome footprints) were isolated and sequenced. To compare the relative density of ribosome footprints on each mitochondrial mRNA between *mtran* mutants and WT, the calculated densities were normalized to both

mRNA length and abundance determined by qRT-PCR (Data S11). As observed in our polysome fractionation analysis, all mitochondrial mRNAs in the *mtran* mutants showed much lower ribosome loading levels compared to WT (Fig. 6A). A single, possibly artefactual, strong footprint observed in *ccmFN<sub>1</sub>* masked the reduction in footprints across the rest of the *ccmFN<sub>1</sub>* mRNA in both *mtran* double mutants. In general, *mtran1-2/2-2* have lower ribosome densities compared to the *mtran1-1/2-1* mutant, especially on mRNAs encoding OXPHOS proteins (~0.5x on average). Visualization of mitoribosome footprints of representative mitochondrial mRNAs clearly showed that translation activity was very low in *mtran1-2/2-2* and moderately low in *mtran1-1/2-1* (Fig. 6B). This shows that not only a subset, but virtually all mitochondrial mRNAs depend on mTRAN proteins for translation, indicating that mTRAN proteins likely are ‘universal’ (for all plant mRNAs) mtSSU subunits involved in translation initiation.

## DISCUSSION

Phylogenetic analysis revealed that mTRANs are likely land plant-specific proteins existing as single-copy genes in most plant-species. Based on the more pronounced growth defects in *mtran1* mutants than *mtran2* mutants, inconsistent detection of mTRAN2 in proteomic studies, and higher mTRAN1 protein number per mitochondrion (3), mTRAN1 is likely the major isoform in Arabidopsis. When *mTRAN1* is knocked out however, *mTRAN2* can apparently take over most functions. When knocking out both isoforms, a range of phenotypes was observed from embryo-lethality (*mtran1-3/2-3*), severe growth defects (*mtran1-2/2-2*), to moderate growth defects (*mtran1-1/2-1*). However, it is not as clear why *mtran1-2/2-2* is (just) viable and *mtran1-3/2-3* is not. We thus propose that *mTRANs* are essential for normal development of plants.

Knocking out *mTRANs* reduced complex I, III, IV and V abundance and activity, while increasing AOX capacity. Because all complexes containing mitochondrially-encoded subunits were strongly reduced in abundance and activity, mTRANs must have a very fundamental function in plant OXPHOS biogenesis. In comparison, mutants in mitochondrial/chloroplast RNA polymerase *rpotmp* are only affected in complex I and IV abundance (32). Together, impaired OXPHOS-dependent ATP production likely causes the growth retardation phenotype in *mtran* mutants. This may be conveyed systemically by negatively affecting e.g. auxin signalling, as observed in the RNA-seq data (Data S4). An antagonistic relation between UPR<sup>mt</sup> and auxin was suggested previously (50) and is underlined by the upregulation of UPR<sup>mt</sup> markers. Downregulation of chloroplast-encoded transcripts by impairing mitochondrial

respiration was also previously reported (32, 51), suggesting an unknown retrograde pathway may reduce chloroplast transcription.

mTRAN1/2 interacted with 17 mtSSU ribosomal proteins. Two proteomic studies also identified mTRAN1/2 as mtSSU components using independent methods (14, 15). Our co-IP additionally identified 5 plant-specific mtSSU rPPR proteins (14, 15). We discovered proteins interacting with mTRANs identified only in our analysis, including *nad7/nad9*, which were less abundant in *mtran* double mutants. We therefore suspect that we captured nascent Nad7/Nad9 peptides that were actively being translated by the mitoribosome. The in organello protein synthesis assays, showing reduced translation rates in the *mtran* double mutants, further support that mTRANs are key mtSSU components required for efficient translation in mitochondria.

Polysome fractionation showed that a much larger proportion of mitochondrial mRNAs is not bound by mitoribosomes in *mtran* double mutants compared to WT, suggesting inefficient translation initiation. The reduced ribosome loading was also observed for *nad6* and *rps4* mRNAs, although Nad6 showed no changes and *rps4* was more abundant at protein level. This suggests that Nad6 protein may be quite stable, possibly even if not incorporated into the fully-assembled complex I. The ribosome fractionation showed that a small fraction of mRNAs (generally <10%) has high ribosome loading in *mtran1-1/2-1* (Fig. 3C), observed in fractions 8-9. We propose that this small fraction of mRNAs could still be bound by the *mtran1-1/2-1* mutant mitoribosomes, perhaps due to different secondary/tertiary structure of the 5' UTR allowing better mitoribosome entry. As a result, these rare 'bindable' mRNAs may then be heavily translated by all available mitoribosomes, partially compensating for the lack of initiation on the vast majority of 'un-bindable' mRNAs. This compensation in the *mtran1-1/2-1* mutant (in which truncated mTRAN1 protein is detected) likely explains the higher vigor of *mtran1-1/2-1* compared to *mtran1-2/2-2* plants.

The question arises as to how mTRAN proteins play such a fundamental role in mitochondrial translation. The polysome fractionation suggests that the problem lies in the very first steps, where the mitoribosome detects and binds the mRNA. Plant mitochondrial mRNAs lack a Shine-Dalgarno (SD) sequence, and plant mitochondrial rRNAs do not have anti-SD sequences (13). Our data suggest that mTRANs are recognition factors, which would mean that in plant mitochondria a protein-mRNA interaction mediates ribosome binding, rather than an rRNA-mRNA interaction. A cryo-EM study of the structure of plant mitoribosomes (16) proposed

that mTRAN1 (named as ms83 and rPPR10 by the authors) is a PPR protein, which are known RNA-binding proteins. Indeed, another study identified mTRAN1 as mRNA-binding protein (52). However, mTRAN proteins are far from ‘classical’ PPR proteins. Firstly, the largest PPR database based on 44,562 PPR protein sequences from >1000 transcriptomes (53, 54) does not identify mTRANs as PPR proteins. Furthermore, ‘TPRpred’ predicts other rPPRs as PPR proteins with 100% confidence, yet only gives a confidence score of 4-14% for mTRAN1/2. Additionally, the gene structure of *mTRAN* with 10 introns is highly aberrant compared to classical PPR genes (Fig. S3A), which usually have 0-1 introns (55). Introns are associated with higher mRNA stability, and indeed *mTRANs* have longer average transcript half-lives of 4.4 h, as compared to 1.7 h for the average PPR gene with 0-1 introns (56), resulting in 1.8-2.4x higher relative expression (Data S12). Nevertheless, only one *mTRAN1* splice form seems dominant, while two are expressed for *mTRAN2* (of which one is low abundant with an early stop codon) according to PastDB (57). However, protein structure prediction tools AlphaFold, RoseTTAFold and iTASSER, showed that mTRAN proteins are likely to have  $\alpha$ -solenoid/PPR protein like-structures (58). Unfortunately, potential RNA-binding sites could not be predicted by aPPRove (43) and PPRCODE (44). This further suggests that mTRAN proteins are  $\alpha$ -solenoid proteins that bind RNA differently to classical PPR proteins. Based on available protein structure predictions, 6-10 repeated motifs were found in the mTRAN protein structure, which suggests they could interact with a mRNA motif of around 6-10 bases, matching our identified CUUUxU/AAGAAx/AxAAA motifs. mTRANs were suggested to sit in a cleft where the incoming mRNA may be positioned in the cryo-EM mitoribosome structure (16). It should be noted that the resolution of several regions in the currently-available plant mitoribosome structure is, however, too low to accurately position mTRANs. Waltz et al (16) hypothesized that mTRAN1 is part of the region that might recognize an AxAAA-related motif of mitochondrial mRNA 5' UTRs, thus acting as a SD–anti-SD-like recognition system. Additionally, their motif analysis suggested that the 5' UTRs of only 17 mitochondrial mRNAs contained a loosely-conserved AxAAA consensus. However, our study showed that mTRANs are required for translation of all mitochondrially-encoded genes, of which many do not contain such an AxAAA 5' UTR motif, but a CUUUxU or AAGAAx motif.

Indeed, mitoribosome loading was lower for all mRNAs in *mtran* mutants. Thus, mTRAN proteins may be “universal” recognition factors for all mitochondrial mRNAs, rather than mRNA-specific initiation cofactors (9, 10). The universally-reduced mitoribosome loading in the *mtran* double mutants is also different from the ribosome loading in *rps10* mutants (59), a

mtSSU subunit thought to be involved in elongation (60). In the *rps10* mutants, variable increased or decreased ribosome loading was observed on mRNAs encoding OXPHOS components, but higher ribosome loading was found for translation- and cytochrome *c* maturation-related mRNAs. This difference further suggests mTRANs are involved in translation initiation, and not elongation.

Most Arabidopsis mitochondrial mRNAs have long 5' UTRs, which is different from mammals but relatively similar to yeast (9). Our results indicate that the putative mitoribosome binding sites CUUUxU and AAGAAx/AxAAAG in plant mitochondrial mRNAs are not at a particular distance from the start codon (Fig. S10 and S11), though with some preference for -25 bases upstream of AUG. Therefore, we hypothesize that either the 2/3D structure of the 5' UTRs may bring the ribosome binding sites physically closer to the start codon, or that plant mtSSU can efficiently scan long 5' UTRs to find the correct AUG, perhaps with the help of other mRNA-specific co-factors (61). In green algae, an A/U-motif is conserved around -25 bases from the start codon (Fig S11), yet mTRAN genes are absent. So perhaps mTRANs evolved in land plants to compensate for increasing variability in mitochondrial ribosome binding site position, or conversely the appearance of mTRANs allowed this variability to occur. These findings indicate that translational initiation by mitochondrial ribosomes occurs in a different way in plants as compared to in fungi and animals (12, 62).

## MATERIALS AND METHODS SUMMARY

Plants were grown under long day condition (16h light/8h dark, approximately 120  $\mu\text{mol photons m}^{-2}\text{s}^{-1}$ ). *A. thaliana* Col-0 was used as WT. The T-DNA insertion lines SALK\_044671, GABI\_915G12, WiscDsLox485-488E21, SALK\_054298, SALK\_096907 and SALK\_099373 were obtained from the European Arabidopsis Stock Centre. The double knockout mutants *mtran1-1/2-1* and *mtran1-2/2-2* were obtained by crossing. Stable transgenic and complementation lines were generated by transforming pB7FWG2-*mTRAN1/2* into WT or *mtran1-2/2-2* by floral dipping, respectively. Plant mitochondria were purified as described in Tran et al (63) for further analysis, e.g. BN-PAGE, western blot, MS/MS analysis, RIP-seq and in organello translation assays. For whole genome RNA-seq analysis, 11-day-old WT and 18-day-old *mtran1-2/2-2* seedlings grown on MS agar plates were harvested at developmental growth stage 1.04 (26). Total RNA was isolated to generate RNA-seq libraries for sequencing. Bioinformatics and statistical analysis were carried out according to Baudry et al (64). Polysomal RNA purified as described in (65) was used for qRT-PCR. mTRAN1 protein was

expressed and purified from *E. coli*. 5'Cy5 labelled RNA probes were obtained from Sigma-Aldrich. REMSAs were performed as described previously (66, 67). Mitoribosome footprints were prepared from Arabidopsis flower buds as previously described (8). Isolated mitochondria from *mito-GFP* and *mTRAN1-GFP* lines were subjected to immunoprecipitations for RIP-Seq analysis as previously described (68). The RIP-seq data was processed, mapped against Col-0 mitogenome, and analysed using DiffSegR to identify mTRAN1-binding sequences. PLMdetect (45) was used to analyze preferred hexameric motif locations in the -300/+200 genomic upstream regions from the start codon of mitochondrial protein-coding genes from all species available in the NCBI database. A complete “Materials and Methods” section is provided in the Supplementary Information.

## REFERENCES

1. O. Schmidt, N. Pfanner, C. Meisinger, Mitochondrial protein import: from proteomics to functional mechanisms. *Nature reviews. Molecular cell biology* **11**, 655-667 (2010).
2. R. S. Rao, F. Salvato, B. Thal, H. Eubel, J. J. Thelen, I. M. Møller, The proteome of higher plant mitochondria. *Mitochondrion* **33**, 22-37 (2017).
3. P. Fuchs, N. Rugen, C. Carrie, M. Elsasser, I. Finkemeier, J. Giese, T. M. Hildebrandt, K. Kuhn, V. G. Maurino, C. Ruberti, M. Schallenberg-Rudinger, J. Steinbeck, H. P. Braun, H. Eubel, E. H. Meyer, S. J. Muller-Schussele, M. Schwarzlander, Single organelle function and organization as estimated from Arabidopsis mitochondrial proteomics. *Plant J* **101**, 420-441 (2020).
4. J. P. Mower, Variation in protein gene and intron content among land plant mitogenomes. *Mitochondrion* **53**, 203-213 (2020).
5. I. M. Møller, A. G. Rasmusson, O. Van Aken, Plant mitochondria - past, present and future. *Plant J*, (2021).
6. N. Mai, Z. M. Chrzanowska-Lightowlers, R. N. Lightowlers, The process of mammalian mitochondrial protein synthesis. *Cell Tissue Res* **367**, 5-20 (2017).
7. B. J. Greber, N. Ban, Structure and Function of the Mitochondrial Ribosome. *Annu Rev Biochem* **85**, 103-132 (2016).
8. N. Planchard, P. Bertin, M. Quadrado, C. Dargel-Graffin, I. Hatin, O. Namy, H. Mireau, The translational landscape of Arabidopsis mitochondria. *Nucleic acids research* **46**, 6218-6228 (2018).
9. K. S. Derbikova, S. A. Levitsky, I. V. Chicherin, E. N. Vinogradova, P. A. Kamenski, Activation of Yeast Mitochondrial Translation: Who Is in Charge? *Biochemistry (Mosc)* **83**, 87-97 (2018).
10. N. S. Green-Willms, T. D. Fox, M. C. Costanzo, Functional interactions between yeast mitochondrial ribosomes and mRNA 5' untranslated leaders. *Mol Cell Biol* **18**, 1826-1834 (1998).
11. J. Montoya, D. Ojala, G. Attardi, Distinctive features of the 5'-terminal sequences of the human mitochondrial mRNAs. *Nature* **290**, 465-470 (1981).
12. E. Kummer, M. Leibundgut, O. Rackham, R. G. Lee, D. Boehringer, A. Filipovska, N. Ban, Unique features of mammalian mitochondrial translation initiation revealed by cryo-EM. *Nature* **560**, 263-267 (2018).
13. T. Hazle, L. Bonen, Comparative analysis of sequences preceding protein-coding mitochondrial genes in flowering plants. *Molecular biology and evolution* **24**, 1101-1112 (2007).
14. N. Rugen, H. Straube, L. E. Franken, H. P. Braun, H. Eubel, Complexome Profiling Reveals Association of PPR Proteins with Ribosomes in the Mitochondria of Plants. *Molecular & cellular proteomics : MCP* **18**, 1345-1362 (2019).
15. F. Waltz, T. T. Nguyen, M. Arrive, A. Bochler, J. Chicher, P. Hammann, L. Kuhn, M. Quadrado, H. Mireau, Y. Hashem, P. Giege, Small is big in Arabidopsis mitochondrial ribosome. *Nat Plants* **5**, 106-117 (2019).
16. F. Waltz, H. Soufari, A. Bochler, P. Giege, Y. Hashem, Cryo-EM structure of the RNA-rich plant mitochondrial ribosome. *Nat Plants* **6**, 377-383 (2020).
17. I. D. Small, N. Peeters, The PPR motif - a TPR-related motif prevalent in plant organellar proteins. *Trends in biochemical sciences* **25**, 46-47 (2000).
18. S. Manna, An overview of pentatricopeptide repeat proteins and their applications. *Biochimie* **113**, 93-99 (2015).
19. C. Schmitz-Linneweber, I. Small, Pentatricopeptide repeat proteins: a socket set for organelle gene expression. *Trends Plant Sci* **13**, 663-670 (2008).

20. A. Moutinho, P. J. Hussey, A. J. Trewavas, R. Malho, cAMP acts as a second messenger in pollen tube growth and reorientation. *Proceedings of the National Academy of Sciences of the United States of America* **98**, 10481-10486 (2001).
21. I. Al-Younis, A. Wong, C. Gehring, The Arabidopsis thaliana K(+)-uptake permease 7 (AtKUP7) contains a functional cytosolic adenylate cyclase catalytic centre. *FEBS letters* **589**, 3848-3852 (2015).
22. N. K. Centeno-Gonzalez, H. I. Martinez-Cabrera, H. Porras-Muzquiz, E. Estrada-Ruiz, Late Campanian fossil of a legume fruit supports Mexico as a center of Fabaceae radiation. *Commun Biol* **4**, 41 (2021).
23. S. A. Rensing, J. Ick, J. A. Fawcett, D. Lang, A. Zimmer, Y. Van de Peer, R. Reski, An ancient genome duplication contributed to the abundance of metabolic genes in the moss *Physcomitrella patens*. *BMC Evol Biol* **7**, 130 (2007).
24. C. M. Hooper, I. R. Castleden, S. K. Tanz, N. Aryamanesh, A. H. Millar, SUBA4: the interactive data analysis centre for Arabidopsis subcellular protein locations. *Nucleic acids research* **45**, D1064-D1074 (2017).
25. J. Senkler, M. Senkler, H. Eubel, T. Hildebrandt, C. Lengwenus, P. Schertl, M. Schwarzlander, S. Wagner, I. Wittig, H. P. Braun, The mitochondrial complexome of Arabidopsis thaliana. *Plant J* **89**, 1079-1092 (2017).
26. D. C. Boyes, A. M. Zayed, R. Ascenzi, A. J. McCaskill, N. E. Hoffman, K. R. Davis, J. Gorlach, Growth stage-based phenotypic analysis of Arabidopsis: a model for high throughput functional genomics in plants. *The Plant cell* **13**, 1499-1510 (2001).
27. G. Karimova, J. Pidoux, A. Ullmann, D. Ladant, A bacterial two-hybrid system based on a reconstituted signal transduction pathway. *Proceedings of the National Academy of Sciences of the United States of America* **95**, 5752-5756 (1998).
28. O. Van Aken, T. Pecenkova, B. van de Cotte, R. De Rycke, D. Eeckhout, H. Fromm, G. De Jaeger, E. Witters, G. T. Beemster, D. Inze, F. Van Breusegem, Mitochondrial type-I prohibitins of Arabidopsis thaliana are required for supporting proficient meristem development. *Plant J* **52**, 850-864 (2007).
29. O. Van Aken, E. Ford, R. Lister, S. Huang, A. H. Millar, Retrograde signalling caused by heritable mitochondrial dysfunction is partially mediated by ANAC017 and improves plant performance. *Plant J* **88**, 542-558 (2016).
30. D. C. Logan, C. J. Leaver, Mitochondria-targeted GFP highlights the heterogeneity of mitochondrial shape, size and movement within living plant cells. *J Exp Bot* **51**, 865-871 (2000).
31. S. M. Kacprzak, A. Dahlqvist, O. Van Aken, The transcription factor ANAC017 is a key regulator of mitochondrial proteotoxic stress responses in plants. *Philosophical transactions of the Royal Society of London. Series B, Biological sciences* **375**, 20190411 (2020).
32. A. Adamowicz-Skrzybowska, M. Kwasniak-Owczarek, O. Van Aken, U. Kazmierczak, H. Janska, Joint inhibition of mitochondrial complex IV and alternative oxidase by genetic or chemical means represses chloroplast transcription in Arabidopsis. *Philosophical transactions of the Royal Society of London. Series B, Biological sciences* **375**, 20190409 (2020).
33. K. Kuhn, G. Yin, O. Duncan, S. R. Law, S. Kubiszewski-Jakubiak, P. Kaur, E. Meyer, Y. Wang, C. C. Small, E. Giraud, R. Narsai, J. Whelan, Decreasing electron flux through the cytochrome and/or alternative respiratory pathways triggers common and distinct cellular responses dependent on growth conditions. *Plant physiology* **167**, 228-250 (2015).
34. M. Kwasniak-Owczarek, A. Tomal, H. Janska, Assessment of Protein Synthesis in Mitochondria Isolated from Rosette Leaves and Liquid Culture Seedlings of Arabidopsis. *Methods in molecular biology* **2363**, 183-197 (2022).
35. R. Kolli, J. Soll, C. Carrie, OXA2b is Crucial for Proper Membrane Insertion of COX2 during Biogenesis of Complex IV in Plant Mitochondria. *Plant physiology* **179**, 601-615 (2019).

36. M. Noll, B. Hapke, M. H. Schreier, H. Noll, Structural dynamics of bacterial ribosomes. I. Characterization of vacant couples and their relation to complexed ribosomes. *Journal of molecular biology* **75**, 281-294 (1973).
37. Y. Fukasawa, J. Tsuji, S. C. Fu, K. Tomii, P. Horton, K. Imai, MitoFates: improved prediction of mitochondrial targeting sequences and their cleavage sites. *Molecular & cellular proteomics : MCP* **14**, 1113-1126 (2015).
38. J. Jumper, R. Evans, A. Pritzel, T. Green, M. Figurnov, O. Ronneberger, K. Tunyasuvunakool, R. Bates, A. Zidek, A. Potapenko, A. Bridgland, C. Meyer, S. A. A. Kohl, A. J. Ballard, A. Cowie, B. Romera-Paredes, S. Nikolov, R. Jain, J. Adler, T. Back, S. Petersen, D. Reiman, E. Clancy, M. Zielinski, M. Steinegger, M. Pacholska, T. Berghammer, S. Bodenstein, D. Silver, O. Vinyals, A. W. Senior, K. Kavukcuoglu, P. Kohli, D. Hassabis, Highly accurate protein structure prediction with AlphaFold. *Nature* **596**, 583-589 (2021).
39. M. Baek, F. DiMaio, I. Anishchenko, J. Dauparas, S. Ovchinnikov, G. R. Lee, J. Wang, Q. Cong, L. N. Kinch, R. D. Schaeffer, C. Millan, H. Park, C. Adams, C. R. Glassman, A. DeGiovanni, J. H. Pereira, A. V. Rodrigues, A. A. van Dijk, A. C. Ebrecht, D. J. Opperman, T. Sagmeister, C. Buhlheller, T. Pavkov-Keller, M. K. Rathinaswamy, U. Dalwadi, C. K. Yip, J. E. Burke, K. C. Garcia, N. V. Grishin, P. D. Adams, R. J. Read, D. Baker, Accurate prediction of protein structures and interactions using a three-track neural network. *Science* **373**, 871-876 (2021).
40. J. Yang, Y. Zhang, I-TASSER server: new development for protein structure and function predictions. *Nucleic acids research* **43**, W174-181 (2015).
41. E. Delannoy, W. A. Stanley, C. S. Bond, I. D. Small, Pentatricopeptide repeat (PPR) proteins as sequence-specificity factors in post-transcriptional processes in organelles. *Biochem Soc Trans* **35**, 1643-1647 (2007).
42. M. R. Karpenahalli, A. N. Lupas, J. Soding, TPRpred: a tool for prediction of TPR-, PPR- and SEL1-like repeats from protein sequences. *BMC bioinformatics* **8**, 2 (2007).
43. T. Harrison, J. Ruiz, D. B. Sloan, A. Ben-Hur, C. Boucher, aPPRove: An HMM-Based Method for Accurate Prediction of RNA-Pentatricopeptide Repeat Protein Binding Events. *PloS one* **11**, e0160645 (2016).
44. J. Yan, Y. Yao, S. Hong, Y. Yang, C. Shen, Q. Zhang, D. Zhang, T. Zou, P. Yin, Delineation of pentatricopeptide repeat codes for target RNA prediction. *Nucleic acids research* **47**, 3728-3738 (2019).
45. J. Rozière, F. Samson, C. Guichard, M. Correa, S. Coursol, M.-L. Martin, V. Brunaud, Plant-PLMview: a database for identifying *cis*-regulatory sequences with preferential positions in gene-proximal regions of plants. *bioRxiv*, 2022.2012.2020.521192 (2022).
46. GitLab, [https://forgemia.inra.fr/GNet/plmdetect/plmdetect\\_tool](https://forgemia.inra.fr/GNet/plmdetect/plmdetect_tool) [accessed 24 May 2023].
47. G. E. Crooks, G. Hon, J. M. Chandonia, S. E. Brenner, WebLogo: a sequence logo generator. *Genome research* **14**, 1188-1190 (2004).
48. A. Liehrmann, E. Delannoy, B. Castandet, G. Rigai, DiffSegR: An RNA-Seq data driven method for differential expression analysis using changepoint detection. *bioRxiv*, 2023.2006.2005.543691 (2023).
49. GitHub, <https://aliehrmann.github.io/DiffSegR/index.html> [accessed 24 May 2023].
50. A. Ivanova, S. R. Law, R. Narsai, O. Duncan, J. H. Lee, B. Zhang, O. Van Aken, J. D. Radomiljac, M. van der Merwe, K. Yi, J. Whelan, A Functional Antagonistic Relationship between Auxin and Mitochondrial Retrograde Signaling Regulates Alternative Oxidase1a Expression in Arabidopsis. *Plant physiology* **165**, 1233-1254 (2014).
51. Y. O. Zubo, T. V. Potapova, V. I. Tarasenko, T. Borner, Y. M. Konstantinov, The rate of transcription in Arabidopsis chloroplasts depends on activity of alternative electron transfer pathway in mitochondria. *Dokl Biochem Biophys* **455**, 76-79 (2014).
52. M. Bach-Pages, F. Homma, J. Kourelis, F. Kaschani, S. Mohammed, M. Kaiser, R. A. L. van der Hoorn, A. Castello, G. M. Preston, Discovering the RNA-Binding Proteome of Plant Leaves with an Improved RNA Interactome Capture Method. *Biomolecules* **10**, (2020).

53. B. Gutmann, S. Royan, M. Schallenberg-Rudinger, H. Lenz, I. R. Castleden, R. McDowell, M. A. Vacher, J. Tonti-Filippini, C. S. Bond, V. Knoop, I. D. Small, The Expansion and Diversification of Pentatricopeptide Repeat RNA-Editing Factors in Plants. *Molecular plant* **13**, 215-230 (2020).
54. Plant Energy Biology (UWA), <https://ppr.plantenergy.uwa.edu.au/> [accessed 10 November 2021].
55. C. Lurin, C. Andres, S. Aubourg, M. Bellaoui, F. Bitton, C. Bruyere, M. Caboche, C. Debast, J. Gualberto, B. Hoffmann, A. Lecharny, M. Le Ret, M. L. Martin-Magniette, H. Mireau, N. Peeters, J. P. Renou, B. Szurek, L. Taconnat, I. Small, Genome-wide analysis of Arabidopsis pentatricopeptide repeat proteins reveals their essential role in organelle biogenesis. *The Plant cell* **16**, 2089-2103 (2004).
56. R. Narsai, K. A. Howell, A. H. Millar, N. O'Toole, I. Small, J. Whelan, Genome-wide analysis of mRNA decay rates and their determinants in Arabidopsis thaliana. *The Plant cell* **19**, 3418-3436 (2007).
57. G. Martin, Y. Marquez, F. Mantica, P. Duque, M. Irimia, Alternative splicing landscapes in Arabidopsis thaliana across tissues and stress conditions highlight major functional differences with animals. *Genome biology* **22**, 35 (2021).
58. D. Fournier, G. A. Palidwor, S. Shcherbinin, A. Szengel, M. H. Schaefer, C. Perez-Iratxeta, M. A. Andrade-Navarro, Functional and genomic analyses of alpha-solenoid proteins. *PloS one* **8**, e79894 (2013).
59. M. Kwasniak-Owczarek, U. Kazmierczak, A. Tomal, P. Mackiewicz, H. Janska, Deficiency of mitoribosomal S10 protein affects translation and splicing in Arabidopsis mitochondria. *Nucleic acids research* **47**, 11790-11806 (2019).
60. S. Hermann-Le Denmat, M. Sipiczki, P. Thuriaux, Suppression of yeast RNA polymerase III mutations by the URP2 gene encoding a protein homologous to the mammalian ribosomal protein S20. *Journal of molecular biology* **240**, 1-7 (1994).
61. N. Haili, N. Planchard, N. Arnal, M. Quadrado, N. Vrielynck, J. Dahan, C. C. des Francs-Small, H. Mireau, The MTL1 Pentatricopeptide Repeat Protein Is Required for Both Translation and Splicing of the Mitochondrial NADH DEHYDROGENASE SUBUNIT7 mRNA in Arabidopsis. *Plant physiology* **170**, 354-366 (2016).
62. V. Singh, J. C. Moran, Y. Itoh, I. C. Soto, F. Fontanesi, M. Couvillion, M. A. Huynen, S. Churchman, A. Barrientos, A. Amunts, Structural basis of LRPPRC-SLIRP-dependent translation by the mitoribosome. *bioRxiv*, 2022.2006.2020.496763 (2022).
63. H. C. Tran, O. Van Aken, Purification of Leaf Mitochondria from Arabidopsis thaliana Using Percoll Density Gradients. *Methods in molecular biology* **2363**, 1-12 (2022).
64. K. Baudry, E. Delannoy, C. Colas des Francs-Small, Analysis of the Plant Mitochondrial Transcriptome. *Methods in molecular biology* **2363**, 235-262 (2022).
65. A. Barkan, Nuclear Mutants of Maize with Defects in Chloroplast Polysome Assembly Have Altered Chloroplast RNA Metabolism. *The Plant cell* **5**, 389-402 (1993).
66. P. Kindgren, A. Yap, C. S. Bond, I. Small, Predictable alteration of sequence recognition by RNA editing factors from Arabidopsis. *The Plant cell* **27**, 403-416 (2015).
67. M. Schallenberg-Rudinger, P. Kindgren, A. Zehrmann, I. Small, V. Knoop, A DYW-protein knockout in Physcomitrella affects two closely spaced mitochondrial editing sites and causes a severe developmental phenotype. *Plant J* **76**, 420-432 (2013).
68. T. T. Nguyen, N. Planchard, J. Dahan, N. Arnal, S. Balzergue, A. Benamar, P. Bertin, V. Brunaud, C. Dargel-Graffin, D. Macherel, M. L. Martin-Magniette, M. Quadrado, O. Namy, H. Mireau, A Case of Gene Fragmentation in Plant Mitochondria Fixed by the Selection of a Compensatory Restorer of Fertility-Like PPR Gene. *Molecular biology and evolution* **38**, 3445-3458 (2021).
69. Y. Perez-Riverol, J. Bai, C. Bandla, D. Garcia-Seisdedos, S. Hewapathirana, S. Kamatchinathan, D. J. Kundu, A. Prakash, A. Frericks-Zipper, M. Eisenacher, M. Walzer, S. Wang, A. Brazma, J. A. Vizcaino, The PRIDE database resources in 2022: a hub for mass spectrometry-based proteomics evidences. *Nucleic acids research* **50**, D543-D552 (2022).

70. ModelArchive, doi/10.5452/ma-9aynd.
71. M. Van Bel, T. Diels, E. Vancaester, L. Kreft, A. Botzki, Y. Van de Peer, F. Coppens, K. Vandepoele, PLAZA 4.0: an integrative resource for functional, evolutionary and comparative plant genomics. *Nucleic acids research* **46**, D1190-D1196 (2018).
72. M. Karimi, D. Inze, A. Depicker, GATEWAY vectors for Agrobacterium-mediated plant transformation. *Trends Plant Sci* **7**, 193-195 (2002).
73. F. Gao, X. Han, J. Wu, S. Zheng, Z. Shang, D. Sun, R. Zhou, B. Li, A heat-activated calcium-permeable channel--Arabidopsis cyclic nucleotide-gated ion channel 6--is involved in heat shock responses. *Plant J* **70**, 1056-1069 (2012).
74. U. Flores-Perez, P. Jarvis, Isolation and Suborganellar Fractionation of Arabidopsis Chloroplasts. *Methods in molecular biology* **1511**, 45-60 (2017).
75. P. Schertl, H. P. Braun, Activity measurements of mitochondrial enzymes in native gels. *Methods in molecular biology* **1305**, 131-138 (2015).
76. A. Cuillerier, Y. Burelle, Hybrid Clear/Blue Native Electrophoresis for the Separation and Analysis of Mitochondrial Respiratory Chain Supercomplexes. *J Vis Exp*, (2019).
77. J. Smet, B. De Paepe, S. Seneca, W. Lissens, H. Kotarsky, L. De Meirleir, V. Fellman, R. Van Coster, Complex III staining in blue native polyacrylamide gels. *J Inherit Metab Dis* **34**, 741-747 (2011).
78. W. Lyu, J. Selinski, L. Li, D. A. Day, M. W. Murcha, J. Whelan, Y. Wang, Isolation and Respiratory Measurements of Mitochondria from Arabidopsis thaliana. *J Vis Exp*, (2018).
79. D. B. Bekker-Jensen, O. M. Bernhardt, A. Hogrebe, A. Martinez-Val, L. Verbeke, T. Gandhi, C. D. Kelstrup, L. Reiter, J. V. Olsen, Rapid and site-specific deep phosphoproteome profiling by data-independent acquisition without the need for spectral libraries. *Nature communications* **11**, 787 (2020).
80. M. C. Chambers, B. Maclean, R. Burke, D. Amodei, D. L. Ruderman, S. Neumann, L. Gatto, B. Fischer, B. Pratt, J. Egerton, K. Hoff, D. Kessner, N. Tasman, N. Shulman, B. Frewen, T. A. Baker, M. Y. Brusniak, C. Paulse, D. Creasy, L. Flashner, K. Kani, C. Moulding, S. L. Seymour, L. M. Nuwaysir, B. Lefebvre, F. Kuhlmann, J. Roark, P. Rainer, S. Detlev, T. Hemenway, A. Huhmer, J. Langridge, B. Connolly, T. Chadick, K. Holly, J. Eckels, E. W. Deutsch, R. L. Moritz, J. E. Katz, D. B. Agus, M. MacCoss, D. L. Tabb, P. Mallick, A cross-platform toolkit for mass spectrometry and proteomics. *Nature biotechnology* **30**, 918-920 (2012).
81. G. K. Smyth, in *Bioinformatics and Computational Biology Solutions Using R and Bioconductor*, R. Gentleman, V. J. Carey, W. Huber, R. A. Irizarry, S. Dudoit, Eds. (Springer New York, New York, NY, 2005), pp. 397-420.
82. R. Gentleman, V. J. Carey, W. Huber, R. A. Irizarry, S. Dudoit, *Bioinformatics and computational biology solutions using R and Bioconductor*. (Springer, 2005), vol. 1.
83. M. E. Ritchie, B. Phipson, D. Wu, Y. Hu, C. W. Law, W. Shi, G. K. Smyth, limma powers differential expression analyses for RNA-sequencing and microarray studies. *Nucleic acids research* **43**, e47 (2015).
84. J. Willforss, A. Chawade, F. Levander, NormalyzerDE: Online Tool for Improved Normalization of Omics Expression Data and High-Sensitivity Differential Expression Analysis. *Journal of proteome research* **18**, 732-740 (2019).
85. D. Chrobok, S. R. Law, B. Brouwer, P. Linden, A. Ziolkowska, D. Liebsch, R. Narsai, B. Szal, T. Moritz, N. Rouhier, J. Whelan, P. Gardestrom, O. Keech, Dissecting the Metabolic Role of Mitochondria during Developmental Leaf Senescence. *Plant physiology* **172**, 2132-2153 (2016).
86. J. R. Wendrich, S. Boeren, B. K. Moller, D. Weijers, B. De Rybel, In Vivo Identification of Plant Protein Complexes Using IP-MS/MS. *Methods in molecular biology* **1497**, 147-158 (2017).
87. C. Carrie, E. Giraud, O. Duncan, L. Xu, Y. Wang, S. Huang, R. Clifton, M. Murcha, A. Filipovska, O. Rackham, A. Vrielink, J. Whelan, Conserved and novel functions for Arabidopsis thaliana

- MIA40 in assembly of proteins in mitochondria and peroxisomes. *The Journal of biological chemistry* **285**, 36138-36148 (2010).
88. B. Zhang, C. Carrie, A. Ivanova, R. Narsai, M. W. Murcha, O. Duncan, Y. Wang, S. R. Law, V. Albrecht, B. Pogson, E. Giraud, O. Van Aken, J. Whelan, LETM proteins play a role in the accumulation of mitochondrially encoded proteins in *Arabidopsis thaliana* and AtLETM2 displays parent of origin effects. *The Journal of biological chemistry* **287**, 41757-41773 (2012).
  89. I. De Clercq, V. Vermeirssen, O. Van Aken, K. Vandepoele, M. W. Murcha, S. R. Law, A. Inze, S. Ng, A. Ivanova, D. Rombaut, B. van de Cotte, P. Jaspers, Y. Van de Peer, J. Kangasjarvi, J. Whelan, F. Van Breusegem, The membrane-bound NAC transcription factor ANAC013 functions in mitochondrial retrograde regulation of the oxidative stress response in *Arabidopsis*. *The Plant cell* **25**, 3472-3490 (2013).
  90. M. Broda, O. Van Aken, Studying Retrograde Signaling in Plants. *Methods in molecular biology* **1743**, 73-85 (2018).
  91. A. M. Bolger, M. Lohse, B. Usadel, Trimmomatic: a flexible trimmer for Illumina sequence data. *Bioinformatics* **30**, 2114-2120 (2014).
  92. S. Gagnot, J. P. Tamby, M. L. Martin-Magniette, F. Bitton, L. Taconnat, S. Balzergue, S. Aubourg, J. P. Renou, A. Lecharny, V. Brunaud, CATdb: a public access to *Arabidopsis* transcriptome data from the URGV-CATMA platform. *Nucleic acids research* **36**, D986-990 (2008).
  93. M. J. del Prete, R. Vernal, H. Dolznig, E. W. Mullner, J. A. Garcia-Sanz, Isolation of polysome-bound mRNA from solid tissues amenable for RT-PCR and profiling experiments. *RNA* **13**, 414-421 (2007).
  94. P. Chotewutmontri, A. Barkan, Multilevel effects of light on ribosome dynamics in chloroplasts program genome-wide and psbA-specific changes in translation. *PLoS genetics* **14**, e1007555 (2018).
  95. D. B. Sloan, Z. Wu, J. Sharbrough, Correction of Persistent Errors in *Arabidopsis* Reference Mitochondrial Genomes. *The Plant cell* **30**, 525-527 (2018).
  96. A. R. Quinlan, I. M. Hall, BEDTools: a flexible suite of utilities for comparing genomic features. *Bioinformatics* **26**, 841-842 (2010).
  97. J. Roziere, C. Guichard, V. Brunaud, M. L. Martin, S. Coursol, A comprehensive map of preferentially located motifs reveals distinct proximal cis-regulatory sequences in plants. *Frontiers in plant science* **13**, 976371 (2022).
  98. B. Langmead, C. Trapnell, M. Pop, S. L. Salzberg, Ultrafast and memory-efficient alignment of short DNA sequences to the human genome. *Genome biology* **10**, R25 (2009).
  99. D. Winter, B. Vinegar, H. Nahal, R. Ammar, G. V. Wilson, N. J. Provart, An "Electronic Fluorescent Pictograph" browser for exploring and analyzing large-scale biological data sets. *PLoS one* **2**, e718 (2007).

## ACKNOWLEDGEMENTS

We thank Dr. Ola Gustafsson for technical assistance for confocal microscopy analysis. We thank Prof. Klas Flärdh for his advice on the cAMP complementation assay. We thank Dr. Malgorzata Kwasniak-Owczarek and Prof. Hanna Janska for their advice on in organello protein synthesis and polysome profiling assays. We thank the POPS platform for the RNA-seq analysis. We thank Ewa Krupinska and Dr. Wolfgang Knecht for their advice on recombinant protein expression. We thank Dr. Peter Kindgren for his advice on REMSAs. We thank Prof. Ian Max Möller for his critical comments on the manuscript. **Funding:** This project was supported by the Swedish Research Council (Vetenskapsrådet 2017-03854; 2021-04358), Crafoord Foundation (20170862; 20190868), Carl Trygger Foundation (CTS 17 487, 22 1981), Kungliga Fysiografiska Sällskapet i Lund and Jörgen Lindström's Foundation, and by grants from the French National Research Agency No. ANR-20-CE11-0021 to H. M. and ANR-20-CE20-0004 to B.C. The POPS platform, the IPS2 and IJPB benefit from the support of Saclay Plant Sciences-SPS (ANR-17-EUR- 0007). **Author contributions:** O.V.A., H.C.T., E.D., H.M. and A.G.R. conceived and planned the project. H.C.T., V.S., S.L., K.B., K.K., A.L-A., B.C, K.H. and C.W. performed experiments. H.C.T., H.M., E.D., C.W., F.L., V.B., A.L. and O.V.A. analyzed data, and. H.C.T. and O.V.A wrote the manuscript with input from all co-authors. **Competing interests:** The authors have no competing interests to declare. **Data and materials availability:** All data are available in the manuscript, supplementary materials or the following repositories. The RNA-Seq project: Gene Expression Omnibus (31) GSE186586. Ribo-seq: ArrayExpress E-MTAB-13059; RIP-Seq: ArrayExpress E-MTAB-13060. The mass spectrometry proteomics data have been deposited to the ProteomeXchange Consortium via the PRIDE (69) partner repository with the dataset identifier PXD043729. The predicted mTRAN structural models are available in ModelArchive (70).

## **SUPPLEMENTARY MATERIALS**

Materials and Methods

Figs. S1 to S12

References (71-99)

Data S1 to S13

**A**

0.1

995

1000

G. max (Glyma.17G023300)

G. max (Glyma.07G251000)

997

1000

S. parvula (Tp3g19500)

A. thaliana mTRAN2 (AT3G21465)

997

1000

A. lyrata (AL3G35540)

1000

S. parvula (Tp7g13890)

A. thaliana mTRAN1 (AT4G15640)

1000

A. lyrata (AL7G39790)

1000

O. sativa (LOC\_Os07g47201)

570

1000

Z. mays (Zm00001d022498)

936

A. trichopoda (ATR0706G238)

P. abies (PAB00014411)

694

872

P. patens (Pp3c14\_15200)

P. patens (Pp3c14\_7470)

M. polymorpha (Mapoly0002s0143)

S. moellendorffii (SMO202G0041)

**B**

GFP MitoTracker Merge

mTRAN1

mTRAN2

**C**

mTRAN1-GFP mTRAN2-GFP

Cyt Mito Cp Cyt Mito Cp

PGRL1

TOM40

GFP

kDa

29

40

70

**D**

Col-0 mtran1-1 mtran1-2

mtran1-3 mtran2-1 mtran2-2

mtran2-3 mtran1-1/2-1 mtran1-2/2-2

**E**

0.1 0.50 0.71 1.0 1.02 1.04

Col-0

mtran1-1

mtran1-2

mtran1-3

mtran2-1

mtran2-2

mtran2-3

mtran1-1/2-1

mtran1-2/2-2

Days after sowing

**F**

25

20

15

10

5

0

15 18 21 24 27 30

Days after sowing

Col-0

mtran1-1

mtran1-2

mtran1-3

mtran2-1

mtran2-2

mtran2-3

mtran1-1/2-1

mtran1-2/2-2

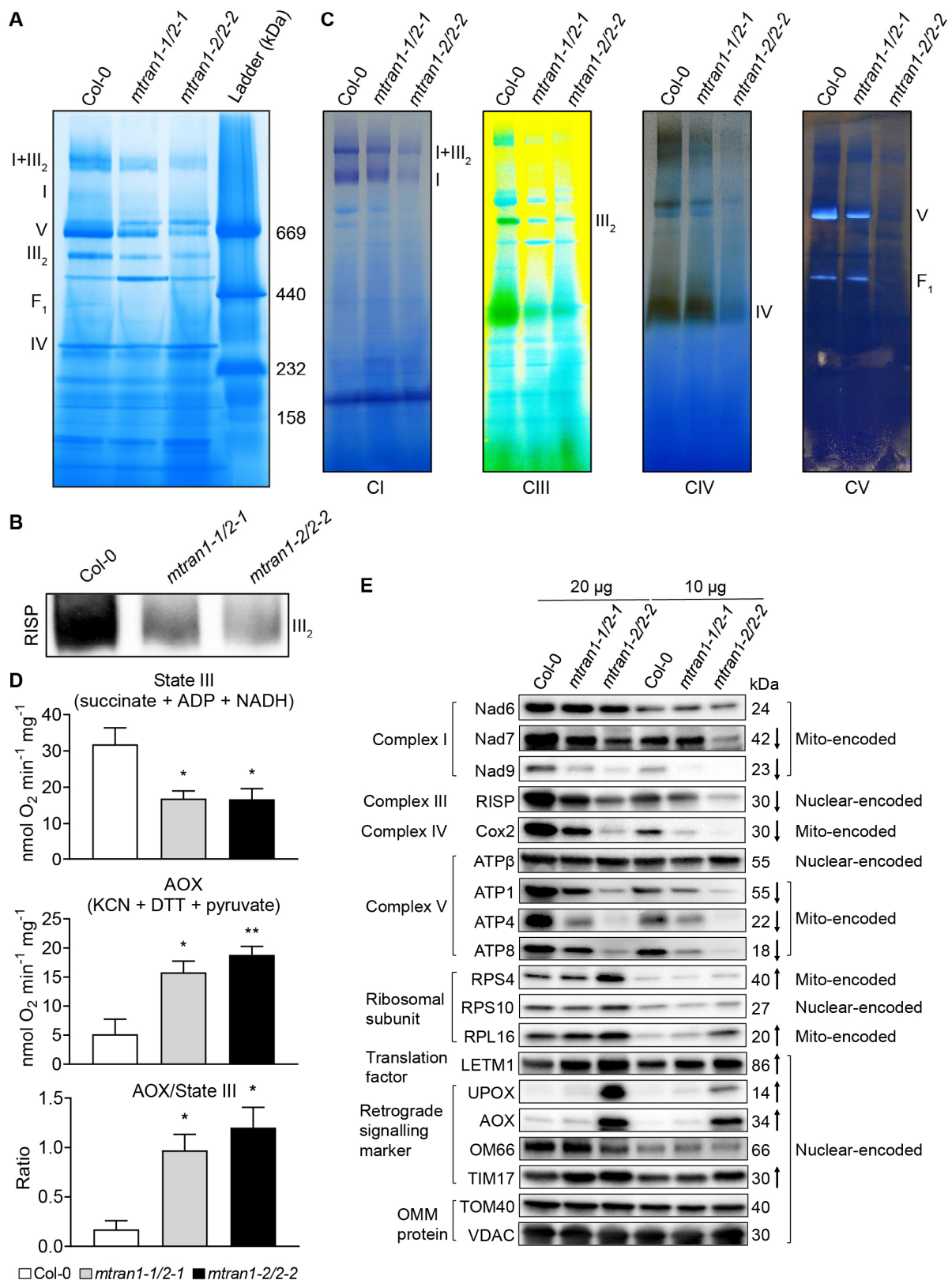
mtran1-1/2-2

mtran1-2/2-3

mtran1-2/2-2

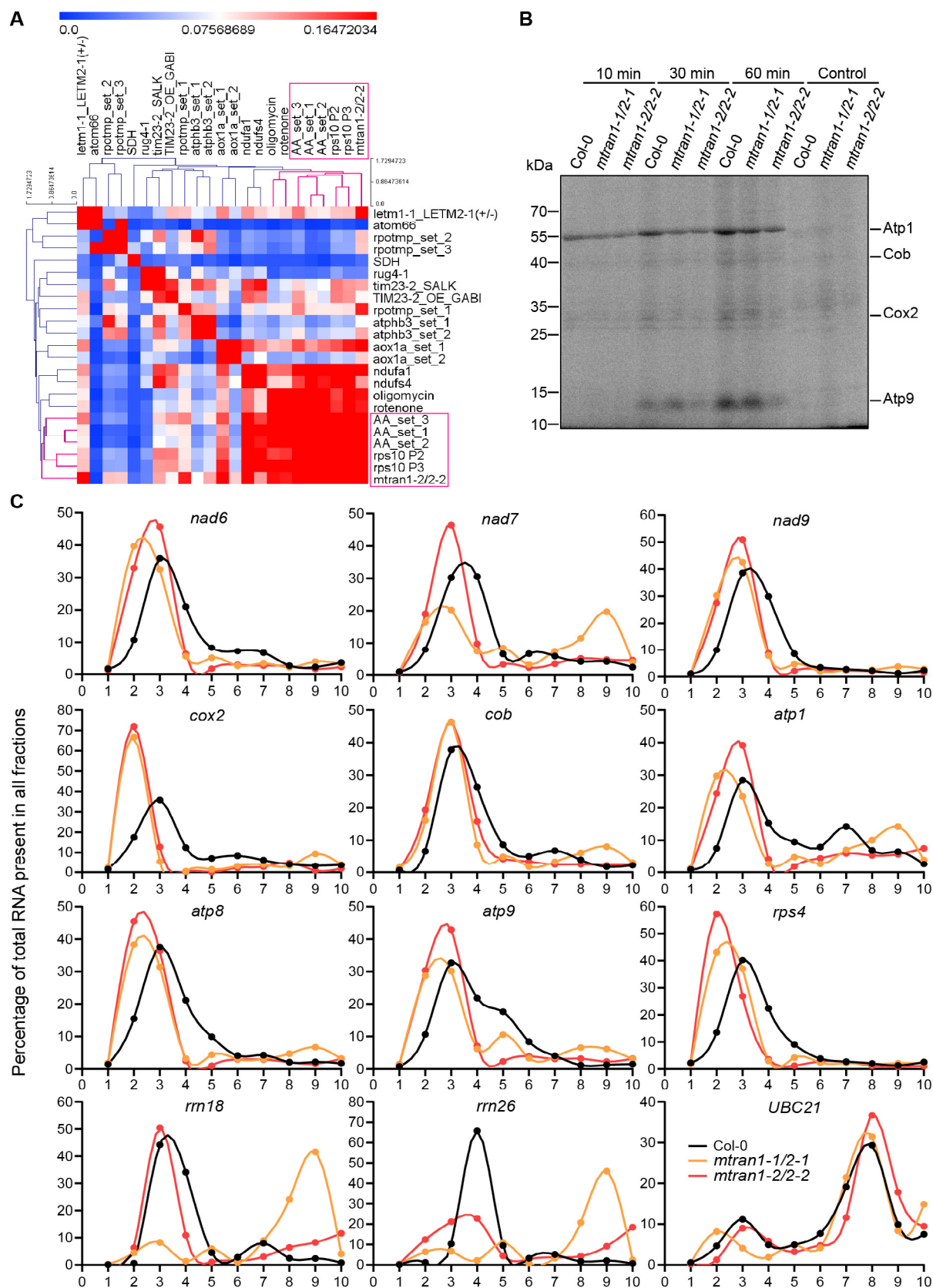
**Figure 1. mTRAN1 and mTRAN2 are land plant-specific mitochondrial proteins required for normal development. A.** Phylogenetic tree of mTRAN1 (AT4G15640) and mTRAN2 (AT3G21465) from *Arabidopsis thaliana* with mTRAN proteins from other

*Embryophyta* (land plants). Scale bar indicates 10% sequence divergence, node numbers indicate bootstrap values. **B.** Full-length coding sequences of mTRAN1 and mTRAN2 were fused with GFP at the C-termini to assess GFP targeting in stably transformed Arabidopsis plants. Imaging was done by confocal microscopy on root cells. Mitochondria were labelled with MitoTracker Red. Scale bars: 5  $\mu$ m. **C.** Immunoblot analysis of cytosolic, mitochondrial and chloroplastic fractions isolated from homozygous Arabidopsis seedlings expressing mTRAN1-GFP and mTRAN2-GFP. Blots were probed with antibodies against chloroplast-targeted PGRL1, mitochondrially targeted TOM40 and GFP. The molecular weight (kDa) is shown on the right side of each blot. Cyt = Cytosol, Mito = Mitochondria, Cp = Chloroplast. **D.** A representative picture of 25-day-old soil-grown plants. Scale bar: 2 cm. **E.** Plate-based phenotypic analysis (means  $\pm$  SD,  $n > 60$ ). Arrows indicate growth stages as described previously (26): 0.1: Seed imbibition; 0.5: Radicle emergence; 0.7: Hypocotyl and cotyledon emergence; 1.0: Cotyledons fully open; 1.02: two rosette leaves  $> 1$  mm; 1.04: four rosette leaves  $> 1$  mm. The boxes indicate the time between the growth stages. **F.** Rosette leaf area of soil-grown plants (means  $\pm$  SD,  $n = 9$ ). Statistical significance was based on Student's *t* test with Bonferroni correction (\*= $P < 0.05$ , \*\*= $P < 0.01$ , \*\*\*= $P < 0.001$ ).



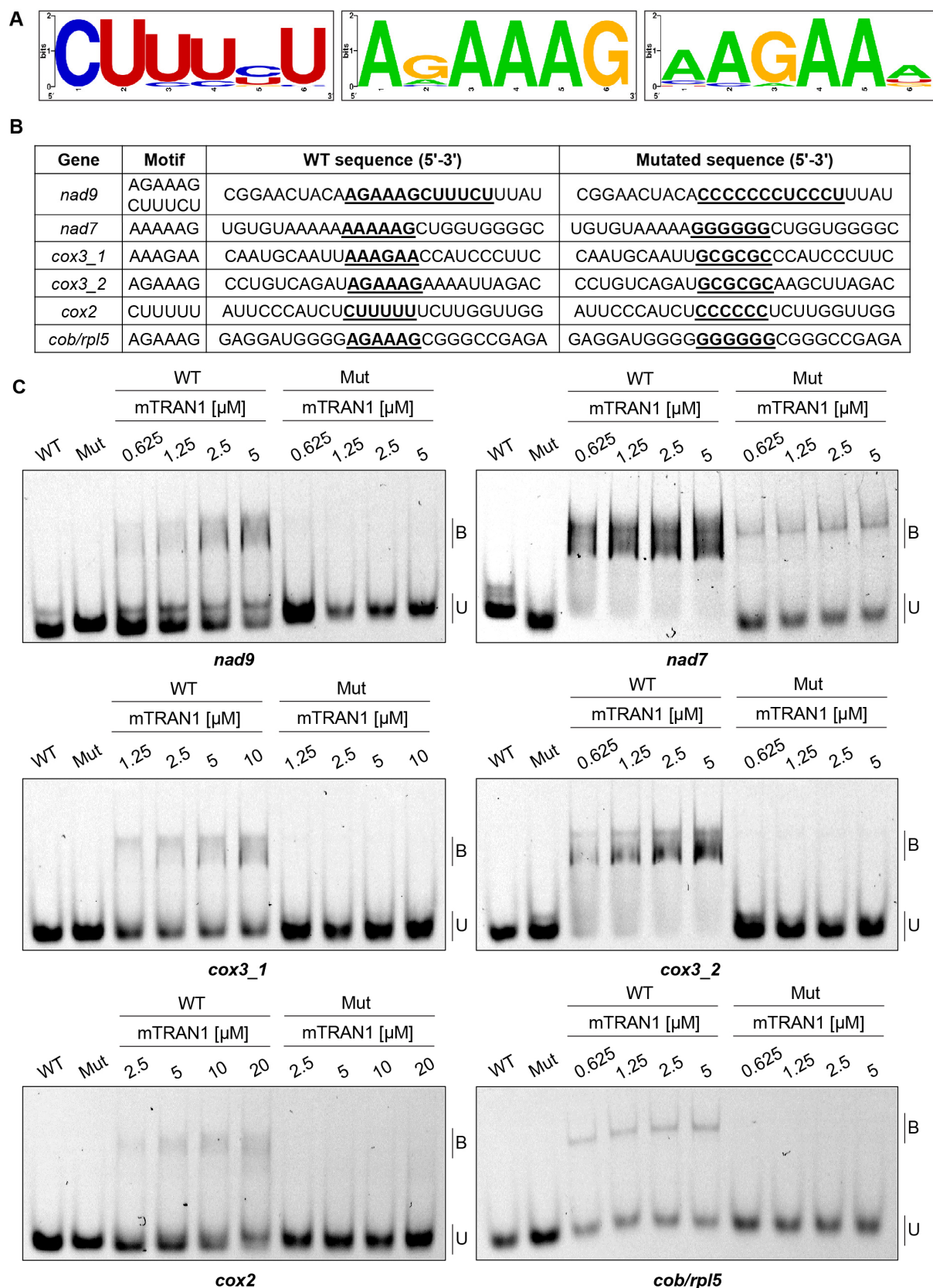
**Figure 2. *mtran* double mutants show defects in mitochondrial biogenesis, protein content and function.** **A.** Analysis of abundance of mitochondrial complexes by Coomassie-Colloidal stained-BN-PAGE. Arrows indicate respiratory complexes and supercomplexes. The molecular weight (kDa) is shown on the right side of the gel. **B.** Western blot using anti-RISP antibody for native complex III on mitochondrial protein extracts of WT and *mtran* double

mutant separated by BN-PAGE. **C.** Activity measurement of the respiratory complexes I, III, IV and V in BN-PAGE. Arrows indicate respiratory complexes and supercomplexes. I+III<sub>2</sub> = supercomplex I+III<sub>2</sub>, CIII=complex III, CIV=complex IV, CV=complex V, F<sub>1</sub>= F<sub>1</sub>-subcomplex of complex V. **D.** Oxygen consumption rates of isolated mitochondria using a Clark-type oxygen electrode. The ratio of maximal AOX respiration/state III respiration = maximized KCN resistant respiration (KCN+DTT+pyruvate)/state III respiration (succinate+ADP+NADH). Statistical significance was based on Student's *t* test (means ± SE, n=3) (\*=*P*<0.05, \*\*=*P*<0.01). **E.** 20 µg and 10 µg of mitochondrial proteins were loaded onto SDS-PAGE for Western Blot analysis. The antibodies and the molecular weight (kDa) are shown on the left and right sides of each blot, respectively. The arrows next to the molecular weight of proteins indicate whether proteins are more abundant (up arrowheads) and less abundant (down arrowheads). Organellar origin of the protein (nuclear-encoded or mitochondrially-encoded) is shown on the right side of the blots. OMM = outer mitochondrial membrane.



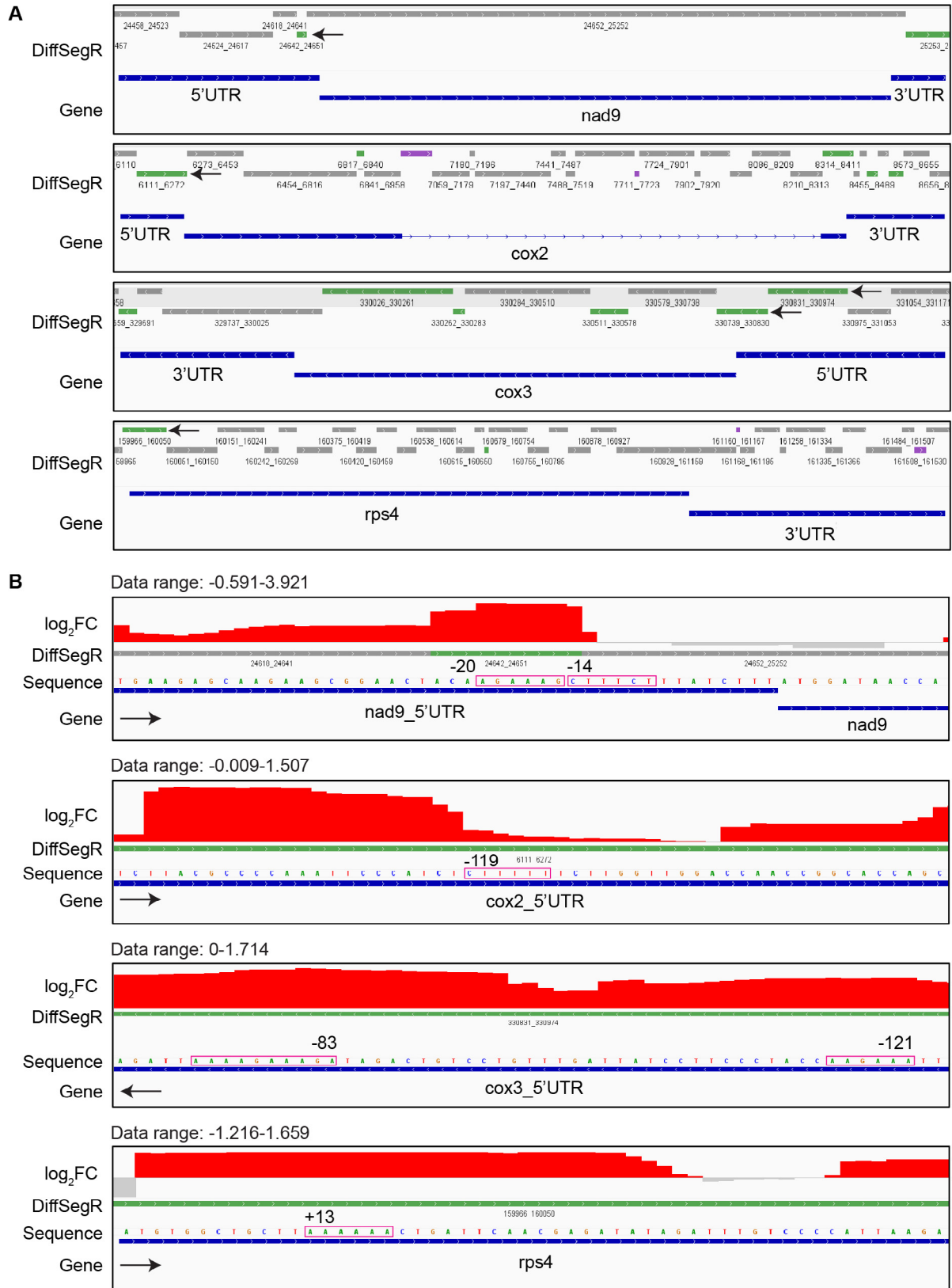
**Figure 3. Loss of mTRAN proteins impairs mitochondrial translation and mitoribosome loading onto mitochondrial mRNAs** A. Heat map representing common pairwise differentially expressed genes (DEGs) among the transcriptomic datasets analysed by the Sørensen-Dice similarity coefficient (DSC). The complete matrix of DSC values for *mtran1*-

2/2-2 and 22 additional datasets was hierarchically clustered using Euclidean Distance. The subbranch including *mtran1-2/2-2* is highlighted for clarity. Color bar indicates linear fold change. **B.** Autoradiogram of in organello protein synthesis for 10, 30 and 60 min using purified mitochondria from WT, *mtran1-1/2-1* and *mtran1-2/2-2*. Sodium acetate was used as substrate to assess bacterial contamination in the controls (60 min). The molecular weight (kDa) and names of identified mitochondrially-encoded proteins are indicated. **C.** Polysome profiling for mitochondrially-encoded transcripts: OXPHOS subunits, mitoribosomal subunit *RPS4* and mitochondrial rRNAs *rrn18/rrn26*, and nuclear-encoded transcript *UBC21*. Percentage of total mRNA in all fractions was measured by qRT-PCR.

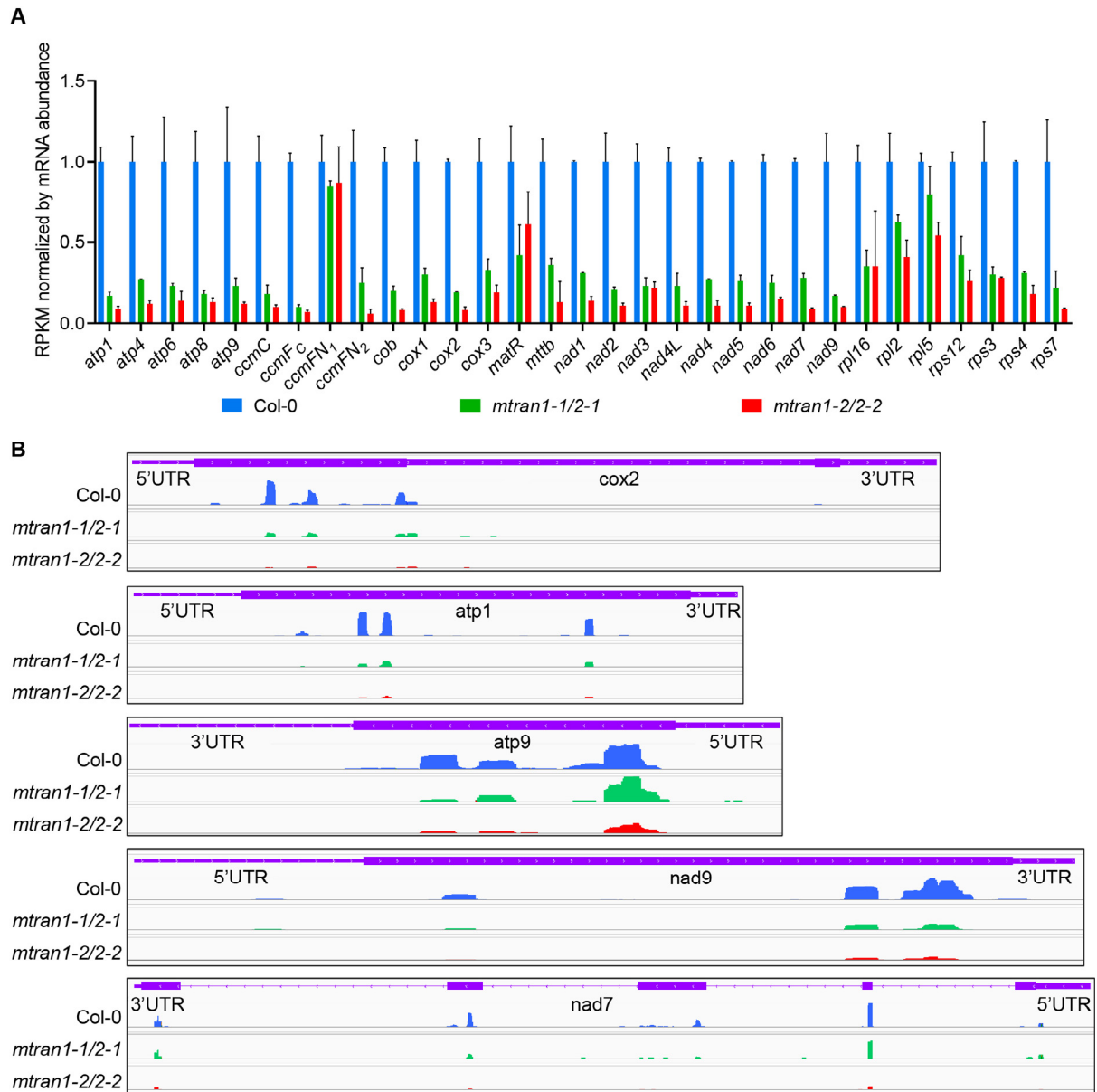


**Figure 4. mTRAN1 binds potential mitoribosome binding sites in vitro.** A. The motif analysis of the 5' UTRs of mitochondrial mRNAs by Multiple Expectation-maximization for Motif Enrichment (MEME) online motif search tool identified potential mitoribosome binding site CUUUXU and AAGAAx. The other potential mitoribosome binding site AxAAAG was

identified by a manual search. The motifs were illustrated with WebLogo (47). **B.** The 5' UTR regions of selected mitochondrial mRNAs containing potential mitoribosome binding sites (underlined) identified by the motif analysis. Binding of recombinantly purified mTRAN1 to the fluorescently-labelled RNA probes was tested by RNA electrophoretic mobility shift assays (REMSAs). The binding sites were specifically changed in the mutated probes (underlined). **C.** REMSAs confirmed the binding of mTRAN1 to the 5' UTRs of mitochondrial mRNAs. Increasing amounts of mTRAN1 were incubated with the RNA probes to allow estimation of the  $K_d$  binding coefficient, according to the indicated concentrations. mTRAN1 had strong specific bindings with *nad9*, *nad7*, *cox3*, *cob/rpl5* and *cox2* that could not be observed when the binding sites were mutated.



control background was calculated by DiffSegR ( $P_{\text{adi}} < 0.05$ ). mTRAN1-specifically bound regions are marked in green (highlighted by black arrows), underrepresented regions in purple and non-enriched regions are marked in gray. The ‘Gene’ track shows the gene structure of the specific genes with untranslated regions (UTR) and coding sequences (CDS). **B.** Close-up of mTRAN1-binding sites in the 5’ UTRs of *nad9*, *cox2*, and *cox3* and in the 5’ end of the *rps4* CDS. Red bar charts indicate  $\log_2\text{FC} > 0$  ( $P_{\text{adi}} < 0.05$ ) obtained by DiffSegR, which represents the mTRAN1-specific immunoprecipitated RNA fragments statistically different from the GFP-control background. The ‘Data range’ indicates minimum and maximum values of the respective  $\log_2\text{FC}$  tracks. The A/U-rich motifs are highlighted for clarity. The positions of the motifs from the start codon AUG are indicated. The black arrows indicate the direction of the genes.



**Figure 6. mTRAN proteins are likely universal mtSSU translation initiation factors. A.** Loss of mTRANs decreases mitochondrial ribosome footprints. Reads per kilobase million (RPKM) normalized by mRNA abundance of the *mtran* double mutants were normalized to WT. Means  $\pm$  SE (n=2). **B.** Density of mitochondrial ribosome footprints on mitochondrially-encoded *cox2*, *atp1*, *atp9*, *nad9* and *nad7* was obtained by Integrative Genomics Viewers (IGV) software using auto-scale.

## Supplementary Materials for

### An mTRAN-mRNA interaction mediates mitochondrial translation initiation in plants

Huy Cuong Tran, Vivian Schmitt, Sbatie Lama, Chuande Wang, Alexandra Launay-Avon, Katja Bernfur, Kristin Sultan, Kasim Khan, Véronique Brunaud, Arnaud Liehrmann, Benoit Castandet, Fredrik Levander, Allan G. Rasmusson, Hakim Mireau, Etienne Delannoy, Olivier Van Aken.

Correspondence to: [olivier.van\\_aken@biol.lu.se](mailto:olivier.van_aken@biol.lu.se)

#### **This PDF file includes:**

Materials and Methods  
Supplementary Text  
Figs. S1 to S12

#### **Other Supplementary Materials for this manuscript include the following:**

Data S1. Mitochondrial proteomic study of the *mtran* double mutants.  
Data S2. Proteins identified as interacting with mTRAN1 and mTRAN2 *in planta*.  
Data S3. RNA-seq analysis of *mtran1-2/2-2*.  
Data S4. Gene ontology analysis of DEGs found in RNA-seq analysis of *mtran1-2/2-2*.  
Data S5. Microarray and RNA-seq datasets used for meta-analysis.  
Data S6. Organellar transcriptome analysis of *mtran1-2/2-2*.  
Data S7. Editing (A) and splicing (B) analysis of mitochondrial transcripts of *mtran1-2/2-2*.  
Data S8. Motif analysis of the 5' UTRs of mitochondrial mRNAs of *Arabidopsis thaliana* using MEME.  
Data S9. Motif analysis of the 5' regions of mitochondrial mRNAs of seed plants (A), liverworts (B), mosses (C) and green algae (D) using PLMdetect.  
Data S10. Motif analysis DiffSegR RIP-seq.  
Data S11. Analysis of mitochondrial ribosome footprints of the *mtran* double mutants.  
Data S12. *mTRAN* mRNA half-life and abundance vs other PPR proteins (0-1 intron).  
Data S13. All oligonucleotides used in this study.

## Materials and Methods

### Phylogenetic analysis

All proteins sequences were collected from PLAZA 4.5 (71). Multiple sequence alignment (MSA) was generated using the algorithm MUSCLE followed by MSA trimming within the PLAZA platform. The edited MSA was used to construct a rooted phylogenetic tree using ClustalX with a bootstrap of 1000 replicates. Node numbers indicate bootstrap values.

### Generation of stable transgenic lines carrying *mTRAN1/2-GFP* and complementation lines *mtran1-2/2-2 mTRAN1/2-GFP*

The full-length coding sequences of *mTRAN1* and *mTRAN2* were amplified by PCR from Arabidopsis Col-0 cDNA. The sequences were cloned into the pDONR221 Gateway vector, then cloned into the 35S binary vector pB7FWG2 (72). Stable transgenic and complementation lines were generated by transforming the constructs into Arabidopsis Col-0 and *mtran1-2/2-2* by floral dipping, respectively. Homozygous transgenic plants were obtained by selecting seeds on half-strength MS agar plates containing 5 mg/mL Basta (glufosinate ammonium, VWR, J66186).

### Subcellular localization

Homozygous plants carrying *35S::mTRAN1-GFP* and *35S::mTRAN2-GFP* were grown on MS agar plates for 7 days. Root tissues of seedlings were harvested just prior to the experiment and incubated with 500 nM MitoTracker<sup>TM</sup> Red CMXRos (M7512, ThermoScientific) for 30 min. *mTRAN1/2-GFP* and MitoTracker-labelled mitochondria were visualized by a confocal laser scanning microscope (Leica SP8 DLS) using excitation wavelengths of 488 nm (*mTRAN1/2-GFP*) and 552 nm (MitoTracker-labelled mitochondria) and emission wavelength of 580 nm for both targets. Subsequent images were captured and processed by LAS X Life Science Microscope Software (Leica).

### T-DNA insertion mutants

T-DNA insertion lines for *mtran1* (SALK\_044671, GABI\_915G12 and WiscDsLox485-488E21) and *mtran2* (SALK\_054298, SALK\_096907 and SALK\_099373) were obtained from the European Arabidopsis Stock Centre. T-DNA insertion homozygous lines were genotyped by standard PCR using the left and right gene-specific primer (LP and RP) and the left border primer of the T-DNA insertion (LB) (Table S13). The genomic position of T-DNA insertion was confirmed by sequencing. The double knockout mutants *mtran1-1/2-1* and *mtran1-2/2-2* were obtained by crossing the single mutants for *mtran1* and *mtran2* as following: SALK\_044671 (*mtran1-1*) x SALK\_054298 (*mtran2-1*), GABI\_915G12 (*mtran1-2*) x SALK\_096907 (*mtran2-2*). Homozygous double mutants were genotyped by PCR.

### Plant growth conditions and phenotyping

All plants were grown under long day condition (16h light/8h dark, approximately 120  $\mu\text{mol photons m}^{-2} \text{ s}^{-1}$ ). Seeds were surface sterilized by liquid sterilization method as described in Tran et al (63). Sterilized seeds were sown on MS agar plates (half-strength MS medium (Duchefa, M0221.0050), 0.05% (w/v) MES (Biomol, 6010.100), 1% (w/v) sucrose (Duchefa, S0809.5000), 0.1% (v/v) Gamborg B5 vitamins (Duchefa, G0415), 0.8% (w/v) phytoagar (Duchefa, P1003.1000), pH 5.7) followed by stratification at 4°C in the dark for 3 days prior to transferring to the growth chamber. Plate-based phenotypic analysis was performed as described in Boyes et al (26). Root length measurement was performed in ImageJ from seedlings grown on vertically placed MS agar plates on day 5, 7 and 9. Seeds sown on soil were also stratified at 4°C in the dark for 3 days prior to transferring to the growth chamber. Measurement of rosette leaf area was performed in ImageJ on day 15, 18, 21, 24, 27 and 30. Data for growth phenotypic analysis was obtained from at least 60 plants/genotype for plate-based phenotypic analysis, 15 plants/genotype for root length measurement, 9 plants/genotype for measurement of rosette leaf area and determination of flowering time.

For mitochondrial purification, sterilized seeds were grown in liquid half-strength MS medium (same ingredients as MS agar medium but without phytoagar) with shaking gently at 100 rpm in long day light condition. Col-0 and *mtran1-1/2-1* were grown for 14 days. As *mtran1-2/2-2* showed a significant growth delay, it was grown for 21 days in total. Therefore, plant material from all genotypes was collected at the same time and all mitochondrial isolations were done on the same day for the sake of giving more consistent results. For in organello protein

synthesis, mitochondria were purified from plants grown in liquid half-strength MS medium supplemented with 50 µg/ml cefotaxime (CAS 64485-93-4) to reduce the risk of bacterial contamination.

#### Bacterial cAMP synthase complementation assay and measurement of cAMP content *in planta*

Bacterial cAMP synthase complementation assay was based on the method of BACTH System kit (Euromedex, France). Full length coding sequences of *mTRAN1* and *mTRAN2* were PCR-amplified from Arabidopsis Col-0 cDNA and then cloned into the vector pUT18. The plasmids were then transformed into the *E. coli* strain *BTH101* and plated on either indicator or selective media to reveal the resulting Cya<sup>+</sup> phenotype as described in the kit protocol. For the positive control, the plasmids pKT25-*zip* and pUT18C-*zip* were co-transformed into *BTH101*. For the negative control, the plasmid pUT18 was transformed into *BTH101*.

For measurement of cAMP content *in planta*, 11-day-old Col-0 and *mtran1-1/2-1* and 18-day-old *mtran1-2/2-2* seedlings grown on MS agar plates were harvested and ground in liquid nitrogen. Measurement of cAMP content *in planta* was performed as described in Gao et al (73). Briefly, 0.4 mL of PBS was added to 0.2 g of ground frozen tissues. After centrifugation at 16100 g at 4°C for 15 min, the supernatant was collected and used to measure cAMP concentration using a cAMP-Glo<sup>TM</sup> assay kit (Promega, V1501) and a plate-reading luminometer (CLARIOstar<sup>Plus</sup>, BMG Labtech) following the kit instructions.

#### Mitochondrial and chloroplastic purification

Mitochondria were purified from 14-day-old plants (Col-0, *mtran1-1/2-1* and homozygous transgenic plants carrying *mTRAN1-GFP* and *mTRAN2-GFP*) and 21-day-old plants (*mtran1-2/2-2*) grown in liquid half-strength MS medium as described in Tran et al (63). For *mTRAN1/2-GFP* plants, the supernatant after the second high-speed centrifugation was collected as the cytosolic fraction. Chloroplasts were isolated from 14-day-old homozygous transgenic plants carrying *mTRAN1-GFP* and *mTRAN2-GFP* grown in liquid half-strength MS medium as described in Flores-Perez et al (74). The concentration of mitochondrial and chloroplastic proteins was determined by Bradford assays (Biorad, 5000006). Isolated mitochondria were used directly for further experimentation requiring intact mitochondria (in organello protein synthesis and measurement of mitochondrial respiration) or stored at -80°C

for later use (BN-PAGE and immunoblotting). Isolated chloroplasts were stored at -80°C for later immunoblot analysis.

#### Analysis of mitochondrial complexes

BN-PAGE using 5% (w/v) digitonin for membrane solubilization was carried out with 500 µg mitochondrial protein per lane as described in Schertl et al (75). Activity measurement of the respiratory complexes I, III, IV and V in BN-PAGE was performed as described previously (75-77).

#### Measurement of mitochondrial respiration

Respiratory measurement of freshly isolated mitochondria was performed using a Clark-type oxygen electrode as described in Lyu et al (78).

#### Analysis of mitochondrial protein abundance by tandem mass spectrometry

Isolated mitochondrial pellets were dissolved in 50 µl of 2% SDS in 100 mM TRIS buffer, pH 7.5 for 30 minutes at room temperature with vortexing at 500 RPM. After centrifugation for 3 min at 13000 RPM, the supernatant was used for reduction and alkylation of proteins using DDT and iodoacetamide. Proteins were loaded to S-Trap columns (ProtiFi, Huntington, NY) and digested with trypsin using the manufacturer instructions with 3 hours digestion. Peptides were eluted, dried in a Speedvac, and stored at -20°C before being desalted on C18 columns (The Nest Group, Ipswich, MA) according to the manufacturer instructions and dried before resuspension in 0.1% formic acid, quantification using Nanodrop and storage at -20°C.

Approximately 400 ng peptides per sample were loaded to Evotips and injected on an Evosep One LC system (Evosep, Odense, Denmark) connected online with a Q-Exactive HF-X Mass Spectrometer (Thermo Fisher Scientific, Germany). Peptides were separated on an EV1109 8 cm column (Evosep) using the 60 SPD method. MS data were acquired in profile mode using data independent acquisition (DIA) with settings essentially as described by Bekker-Jensen et al (79) with one full MS scan 350-1400 m/z followed by 49 windows DIA with an isolation

widths of 13.7 m/z and evenly distributed window centers from 471.5 to 1129.1 m/z. For full MS scans AGC target was 3e6, resolution 120000 and maximum injection time 25 ms. For DIA scans AGC target was 3e6, target resolution 15000, maximum injection time 22 ms and normalized collision energy 27.

Raw data files were converted to mzML using Proteowizard version 3.0.21098 (80) with vendor peakpicking enabled. The mzML files were processed in DIA-NN version 1.8 in library free mode against the UniProt *Arabidopsis thaliana* proteome UP000006548 downloaded on 10<sup>th</sup> February 2022. In DIA-NN enzymatic cleavage was set after KR with maximum one missed cleavage and cystein carbamidomethylation was set as fixed modification and N-terminal methionine excision as variable modification. Two pass search (match between runs) was enabled with automated mass accuracy estimation and other settings were set to default.

The protein groups matrix file from DIA-NN was used for data analysis. Normalization of quantitative values with Cyclic Loess normalization (81, 82) and differential abundance analysis using LIMMA (83) were performed in NormalyzerDE version 1.14.0 (84). List of *Arabidopsis* mitochondrial proteins were based on previous studies (24, 85).

#### Co-immunoprecipitation followed by tandem mass spectrometry

Homozygous transgenic plants carrying *mTRAN1-GFP* and *mTRAN2-GFP* generated as described above were grown on half-strength MS agar plates for 11 days. Seedlings were harvested and ground in liquid nitrogen. 3 g of powdered plant material was used per replicate. Co-immunoprecipitation was performed as described in Wendrich et al (86). The pH of the protein samples was adjusted to 7.8 before being reduced by DTT (CAS 27565-41-9) to a final concentration of 5 mM. The protein samples were incubated in 37°C for 30 min, followed by alkylation by adding iodoacetamide to a final concentration 12 mM and incubation in the dark for 20 min. The samples were digested by addition of sequencing-grade modified trypsin (Promega, Madison, WI, USA) to a final concentration 2 ng/μl and incubation overnight at 37 °C. Formic acid was added to the digested samples and the supernatant containing the peptides was collected by centrifugation at 15000 g for 10 min. For tandem mass spectrometry, the peptides were cleaned up on C18 reversed phase micro columns and subjected to reversed phase nano-LC source (Proxeon Biosystems) coupled to an LTQ-Orbitrap Velos Pro mass spectrometer equipped with a nano Easy spray ion source (ThermoScientific). Identification of proteins were carried out with the Mascot Daemon software (version 2.4) and searched against

the Arabidopsis database TAIR. To be considered as a true protein identification, all individual ion scores must have a higher score than the score given when using a significant threshold of  $p < 0.005$ .

#### In organello protein synthesis

In organello protein synthesis was performed as described in Kwasniak-Owczarek et al (34). Briefly, 300  $\mu\text{g}$  of freshly isolated mitochondria was resuspended in the translation mix containing 5 mM  $\text{KH}_2\text{PO}_4$ , pH 7.0, 2 mM GTP, 0.4 M mannitol, 60 mM KCl, 2 mM DTT, 50 mM HEPES, 10 mM  $\text{MgCl}_2$ , 10 mM malic acid, 1 mM pyruvate, 4 mM ADP, 0.1% (w/v) BSA, 25 mM unlabelled 19-amino acid solution (Promega), and 30  $\mu\text{Ci}$  [ $^{35}\text{S}$ ]Met ( $>1000$  Ci/mmol, SRM-01H, Hartmann Analytic). For the control, 25 mM Na-acetate was used instead of malic acid and pyruvate. To inhibit potential contamination of chloroplast and cytoplasmic ribosomes, erythromycin and cycloheximide were added to all reactions to a final concentration of 200  $\mu\text{M}$  and 100  $\mu\text{M}$ , respectively. Reactions were carried out in 100  $\mu\text{l}$  for 10, 30 and 60 min at room temperature on an orbital shaker and stopped by adding 350  $\mu\text{l}$  mitochondria wash buffer (without BSA) containing 10 mM unlabelled L-methionine and puromycin (50  $\mu\text{g}/\text{mL}$ ). Radiolabelled proteins were separated by SDS-PAGE and detected by autoradiography.

#### Immunoblotting of mitochondrial and chloroplastic proteins

Isolated chloroplastic proteins (10  $\mu\text{g}$ ) and isolated mitochondrial proteins (10  $\mu\text{g}$  and 20  $\mu\text{g}$ ) were separated by SDS-PAGE and transferred to a PVDF membrane using the Trans-Blot Turbo Mini PVDF Transfer Pack (Biorad) and the Trans-Blot Turbo Transfer System (Biorad). Blots were probed with the primary antibodies against the subunits of OXPHOS: NAD6 (PHY1079S), NAD7 (PHY1077S), NAD9 (PHY0516S), COX2 (PHY1413S), ATP1 (PHY2146S), ATP4 (PHY1129S) and ATP8 (PHY1130S) from PhytoAB (U.S.A); RISP from Carrie et al (87); ATP $\beta$  and PGRL1 from Agrisera (Sweden); and GFP from Thermo Fisher Scientific (U.S.A). Blots were also probed with the primary antibodies against mitoribosomal proteins RPS4, RPS10 and RPL16 (Agrisera) that were kindly provided by Prof. Hanna Janska (University of Wroclaw, Poland); mitochondrial translation factor LETM1 (88); mitochondrial retrograde signalling markers UPOX and AOX (89); IMM proteins OM66 and TIM17, and

OMM proteins TOM40 and VDAC from Prof. James Whelan (La Trobe University, Australia). Anti-rabbit antibodies conjugated with horseradish peroxidase (HRP) were used as secondary antibodies, except for AOX and VDAC, an anti-mouse antibody-HRP was used. Chemiluminescence was detected by using Clarity Western ECL Substrate (Biorad) and the ChemiDoc XRS+ System (Biorad).

### qRT-PCR

Total RNA was extracted from 11-day-old Col-0 and *mtran1-1/2-1* seedlings and 18-day-old *mtran1-2/2-2* seedlings grown on MS agar plates using the Spectrum™ Plant Total RNA Kit (Sigma Aldrich, STRN250-1KT, DNASE70-1set). cDNA synthesis and qRT-PCR was performed as described in Broda et al (90) using the iScript™ cDNA Synthesis Kit (Biorad, 1708891) and CFX384 Real-time PCR Detection System (Biorad) using Sso Advanced Universal SYBR green detection assays (Biorad, 172-5271), respectively. The nuclear gene *UBIQUITIN-CONJUGATING ENZYME 21 (UBC21)* was used for data normalization. Transcripts were measured in technical duplicate from three independently biological replicates. All primers are listed in Data S13.

### RNA-seq analysis

11-day-old Col-0 and 18-day-old *mtran1-2/2-2* seedlings grown on MS agar plates were harvested at developmental growth stage 1.04 (26). Each sample was composed of 4-5 seedlings (approximately 50 mg fresh weight). Three biological replicates of Col-0 and *mtran1-1/2-1* were analyzed. Total RNA was extracted using the Spectrum™ Plant Total RNA Kit (Sigma Aldrich) according to the supplier's instructions and was further purified using the RNA Clean & Concentrator Kits (Zymo Research®, California, U.S.A.). RNA-seq libraries were constructed by the POPS platform (IPS2) using the TruSeq Stranded Total RNA kit with Ribozero Plant (Illumina®, California, U.S.A.) according to the supplier's instructions. The libraries were sequenced in single-end (SE) mode with 75 bases for each read on a NextSeq500. Adapter sequences and bases with a Q-Score below 20 were trimmed out from reads using Trimmomatic (v0.36, Bolger et al (91)) and reads shorter than 30 bases after trimming were discarded. After trimming, between 57 and 84 million of SE reads per sample were obtained. The bioinformatics and statistical analysis were carried out using pipelineOGE available at

<https://forgemia.inra.fr/GNet/pipelineoge> (64). All steps of the experiment, from growth conditions to bioinformatic analyses, were detailed in CATdb (92): <http://tools.ips2.u-psud.fr.fr/CATdb/> according to the MINSEQE "minimum information about a high-throughput sequencing experiment".

### Meta-analysis of transcriptome datasets

A full list of the transcriptome datasets of *mtran1-2/2-2* and 22 additional Arabidopsis mitochondrial mutants and chemical treatments affecting mitochondrial function can be found in Table S5. Transcripts were considered to be significantly differentially expressed if  $ppde.p > 0.95$  or  $P_{adj} < 0.05$  (after False Discovery Rate correction) with two-fold change. The similarities among all datasets were evaluated by comparison of common pairwise DEGs calculated via the Sørensen-Dice similarity coefficient (DSC) with formula  $DSC(a,b) = 2n_{ab}/(n_a + n_b)$ . Therefore, the DSC between two datasets ranges from 0 to 1. The complete matrix of DSC values for *mtran1-2/2-2* and 22 additional datasets was hierarchically clustered in TIGR Multi-experiment Viewer 4.9.0 using Euclidean Distance and represented as a heat map.

### Purification of polysomal RNA

Polysomal RNA from 11-day-old Col-0 and *mtran1-1/2-1* seedlings and 18-day-old *mtran1-2/2-2* seedlings grown on MS agar plates was purified as described in Barkan (65) with modifications. 1 mL of polysome extraction buffer (0.2 M Tris-HCl, pH 9.0, 0.2 M KCl, 35 mM MgCl<sub>2</sub>, 25 mM EGTA, 0.2 M sucrose, 1% v/v Triton X-100, 2% v/v Polyoxyethylene-10-tridecyl ether, 0.5 mg/ml heparin, 100 mM 2-mercaptoethanol, 100 µg/ml chloramphenicol and 25 µg/ml cycloheximide) was added to 0.2 g of ground frozen tissues and the sample was vortexed until thawed. Debris from extraction was removed by centrifugation at 4°C and max speed for 1 min and filtered through a QIAshredder column (Qiagen). The sample was incubated on ice for 10 min to solubilize membranes and centrifuged at 4°C and max speed for 5 min. Sodium deoxycholate was added to the supernatant to a final concentration of 0.5% w/v. The sample was incubated on ice for 5 min to complete microsomal membrane solubilization and centrifuged at 4°C and max speed for 15 min to pellet insoluble material. The supernatant (450 µl) was layered onto 4 ml sucrose gradients (55:40:30:15% w/v sucrose in 40 mM Tris-HCl, pH 8.0, 20 mM KCl, 10 mM MgCl<sub>2</sub>, 100 µg/ml chloramphenicol, 0.5 mg/mL heparin and 25 µg/ml cycloheximide) and fractionated by ultracentrifugation (SW50.1 rotor, 4°C, 45000 rpm, 65 min). After that, 10 fractions (~445 µl each) were collected from the top of the gradient

and subjected to total RNA isolation using phenol/chloroform/isoamyl (25:24:1) (Sigma Aldrich). Isolated RNA from all fractions were treated with 2.5 M LiCl to remove the heparin as described previously (93). The same volume of RNA from each fraction was used for cDNA synthesis and qRT-PCR as described above.

#### Ribo-Seq library preparation and sequencing

Mitoribosome footprints were prepared from Arabidopsis flower buds as previously described with two samples per genotype (8). Ribosome footprints were depleted from ribosomal RNAs after first strand cDNA synthesis using custom biotinylated oligonucleotides matching major rRNA contaminants found in previous experiments (8). Ribo-Seq libraries were prepared using the TruSeq Small RNA library preparation kit (Illumina). Next generation sequencing was performed on a NovaSeq6000 instrument (Illumina) using a SP-100 flowcell and a single end 75 nt pass. Mitochondrial mRNA abundances were determined by RT-qPCR using the same set of primers described in Planchard et al (8).

#### Ribo-Seq Bioinformatic analyses

Ribo-Seq sequencing data were processed and mapped as previously described in Planchard et al (8). Ribo-Seq RPKMs were calculated based on reads mapping to mitochondrial and nuclear coding sequences following a procedure detailed in Chotewutmontri et al (94) and translation efficiencies were calculated as ratios of ribosome footprint RPKMs to mRNA abundances determined by RT-qPCR.

#### Predicted protein structure of mTRAN1 and mTRAN2

Protein sequences of mTRAN1 and mTRAN2 lacking their MTS predicted by MitoFates (<http://mitf.cbrc.jp/MitoFates/cgi-bin/top.cgi>) (37) were used for protein structure prediction tools AlphaFold (ColabFold: AlphaFold2 using MMseqs2 <https://colab.research.google.com/github/sokrypton/ColabFold/blob/main/AlphaFold2.ipyn>) (38), RoseTTAFold (<https://robetta.bakerlab.org/>) (39) and iTASSER (<https://zhanggroup.org/I-TASSER/>) (40). The PPR codes of mTRAN1 and mTRAN2 were

searched in aPPRove (43) and PPR Code Prediction Web Server <http://yinlab.hzau.edu.cn/pprcode/> (44).

#### Motif analysis of the 5' UTRs of mitochondrial mRNAs of *Arabidopsis thaliana*

The sequences of the 5' UTRs of mitochondrial transcripts were based on the recently re-annotated *Arabidopsis thaliana* ecotype Col-0 mitochondrial genome (NC\_037304) (95). Briefly, coordinates corresponding to the 5' UTRs were used to retrieve the corresponding sequences using BEDTools (command “getfasta”) (96). If the transcript contained several alternative overlapping 5' UTRs, the longest 5' UTR was selected. The 5' UTRs of fully spliced transcripts, which are upstream of the first exons, were selected in case of trans-spliced transcripts *NAD1*, *NAD2* and *NAD5*. Because the mitochondrial genome contains polygenic transcriptional units, some distinct genes share the same 5' UTRs, for example, *NAD4L* and *ATP4*, *RPL5* and *COB*, *NAD3* and *RPS12*. There is also some suggestion that the second gene in polycistronic mRNAs may have its own 5' UTR and ribosome binding site in between the two genes, but these are not defined. Therefore, we analysed the collection of mitochondrial 5' UTRs both with and without these putative inter-cistronic 5' UTRs. The motif analysis of mitochondrial mRNA's 5' UTRs was performed using Multiple Expectation-maximization for Motif Enrichment (MEME) online motif search tool (site distribution: any number of repetitions; motif width: 6-10) and identified a potential mitoribosome binding site CUUUxU and AAGAAx. The MEME motif search tool was unable to identify the AxAAA-related motif, but a AxAAA-like motif, AxAAAG, was manually searched in the 5' UTRs of mitochondrial mRNAs.

#### Motif analysis of upstream sequences of mitochondrial mRNAs of seed plants, liverworts, mosses and green algae

Mitogenome sequences (fasta files) and gene annotations (gff3 files) from 1983 seed plants, 114 mosses, 60 liverworts and 309 green algae species were extracted from the NCBI database in March 2023. The genomic sequences from -1300 to +200 relative to the ATG of all protein coding sequences were then extracted using custom bash/perl scripts and bedtools (96). The preferential position of all possible 6-base motifs from -300 to +200 relative to the ATG was identified using PLMdetect (97) for 49706 seed plant mitogenes, 4256 moss mitogenes, 2569

liverwort mitogenes and 7867 green algae mitogenes (Table S9). For each motif, PLMdetect compares its frequency at each position of the distal region (-1300 to -300) to its frequency at each position of the proximal region (-300 to +200) to identify positions with significantly higher frequency. In the proximal region, the density of preferentially located motifs (PLM) was calculated as the sum, for all PLMs preferentially located at this position, of all genes with these PLMs. To compare between the different groups, the values were divided by the maximum value along this segment.

The logos were generated from the list of PLMs present at -1 to +1 of the position of interest using WebLogo (v2.8.2) (47) and the contribution of each motif to the logo was weighted by their frequency.

#### Recombinant protein purification and REMSAs

pET-26b(+)-*His-SUMO3-mTRAN1* plasmid with codon optimization was obtained from GeneScript (U.S.A). The plasmid was expressed in *E. coli* Tuner DE3 by IPTG induction to a final concentration of 1 mM at OD<sub>600</sub> = 0.6-0.8 at 18°C for 20 hours. Protein purification was performed using GE Healthcare HisTrap FF columns (17-5247-01) according to the manufacturer's instructions. Purified His-SUMO3-mTRAN1 was digested with SenP2 (enzyme:substrate ratio of 1:35) to remove the tag His-SUMO3. The His-SUMO3-mTRAN1/SenP2 mixture was transferred to a dialysis membrane (SpectraPor, MWCO 3500) and was dialyzed against 2 L of wash buffer including 1 mM DTT at 4°C overnight with stirring. On the next day, the mixture was taken from the dialysis membrane, filtered (0.45 µm) and loaded on a GE Healthcare HisTrap FF column to collect the flow-through containing the mTRAN1 protein without affinity tag. Purified protein concentrations were determined by Bradford assays (Biorad). 5'Cy5 labelled probes were obtained from Sigma Aldrich. REMSAs were performed as described previously (66, 67) with modifications. Briefly, reactions consisting of 10 µl 2x binding buffer (2.5x THE, 40 µg/ml BSA, 5 mM DTT, 0.5 mg/ml Heparin (Sigma-Aldrich, H4784), 200 mM NaCl), 10 µl purified protein and 5 µl RNA probe (1 nM final concentration) were incubated at 25°C for 15 min and loaded onto a pre-run 5% native gel in 1x THE (34 mM Tris, 66 mM HEPES, 0.1 mM EDTA pH=8) that was run at 4°C. The gels were imaged with a Typhoon 9500 (GE Healthcare).

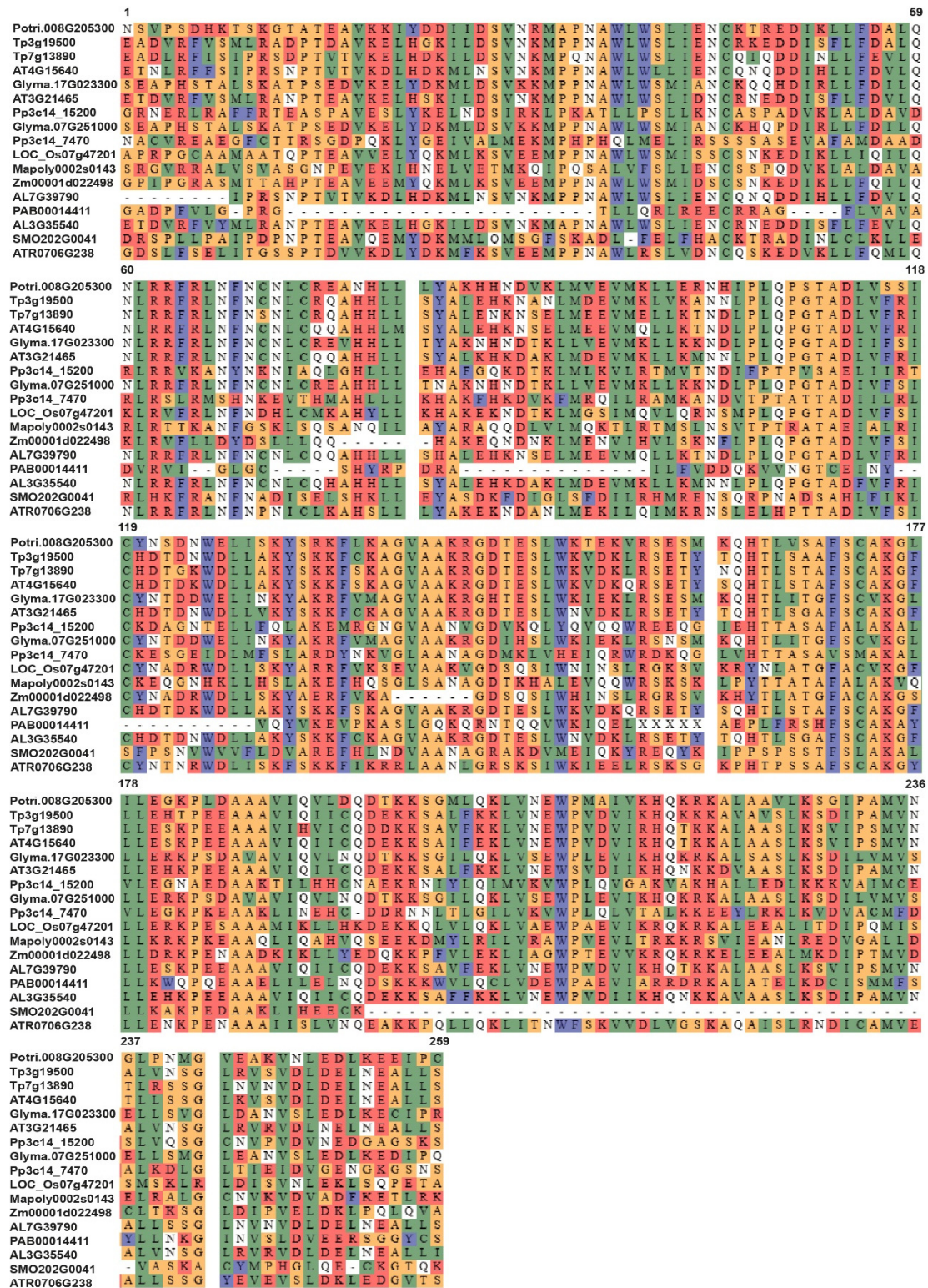
## RIP-Seq

Isolated mitochondria from *mTRAN1-GFP* and *mito-GFP* lines were used for RIP-seq analysis using anti-GFP antibodies in duplicates per genotype, which were performed as previously described in detail by Nguyen et al (68). RIP-seq libraries were prepared using the TruSeq Small RNA library preparation kit (Illumina) as previously described in Nguyen et al (68). Next generation sequencing was performed on a NextSeq2000 instrument (Illumina) using a P2 flow cell and a single end 130+6 nt pass. Raw reads were processed with cutadapt v2.10 (DOI:10.14806/ej.17.1.200) to remove adapters and then mapped onto the *A. thaliana* genome including the Col-0 mitogenome (95) using bowtie (v1.2.2) (98) with the parameter -v 1.

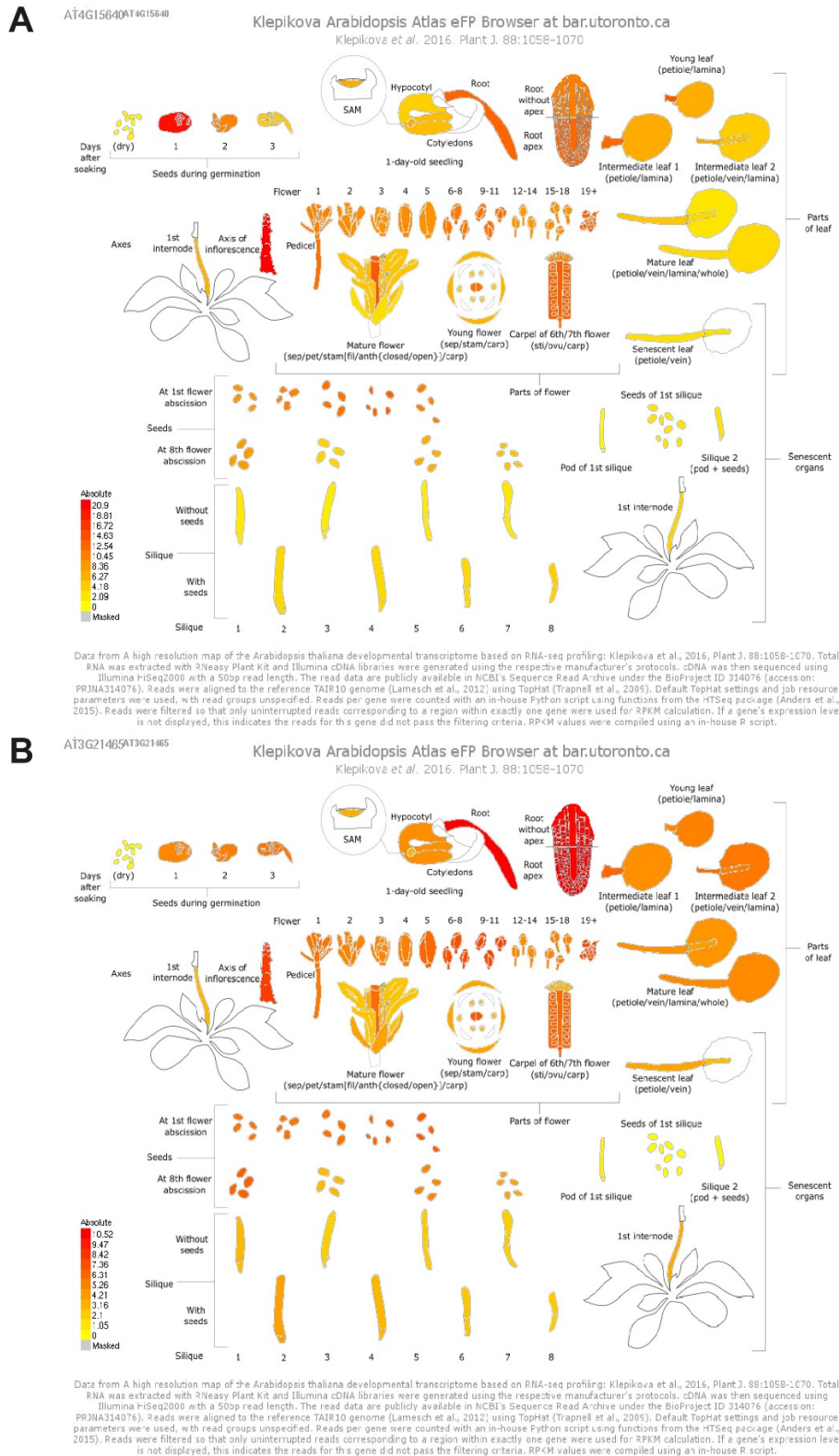
The differential expression analyses across the mitochondrial genome between *mito-GFP* and *mTRAN1-GFP* RIP-Seq data were performed utilizing the DiffSegR R package v.1.0 (<https://aliehrmann.github.io/DiffSegR/index.html>) (48). This package employs a multiple changepoints detection algorithm, which is designed to accurately pinpoint the boundaries of potential differentially expressed regions in the per-base log<sub>2</sub> fold change (log<sub>2</sub>FC) signal. Following the identification of these regions, each one is subjected to rigorous statistical evaluation using the DESeq2 R package v.1.34.0. Finally, the results are exported in IGV v.2.14.1. The per-base log<sub>2</sub>FC calculations were performed by DiffSegR by setting the coverageType parameter to "fullLength" within the loadData function. To mitigate the impact of spurious changepoints, we enhanced the alpha parameter to 32 within the segmentation function. Following the differential assessment with DESeq2, only regions demonstrating an adjusted p-value of less than 0.05 (BH) were deemed statistically significant. The DiffSegR outputs for viewing in IGV can be downloaded from <https://doi.org/10.57745/A62BMV>.

## Accession numbers

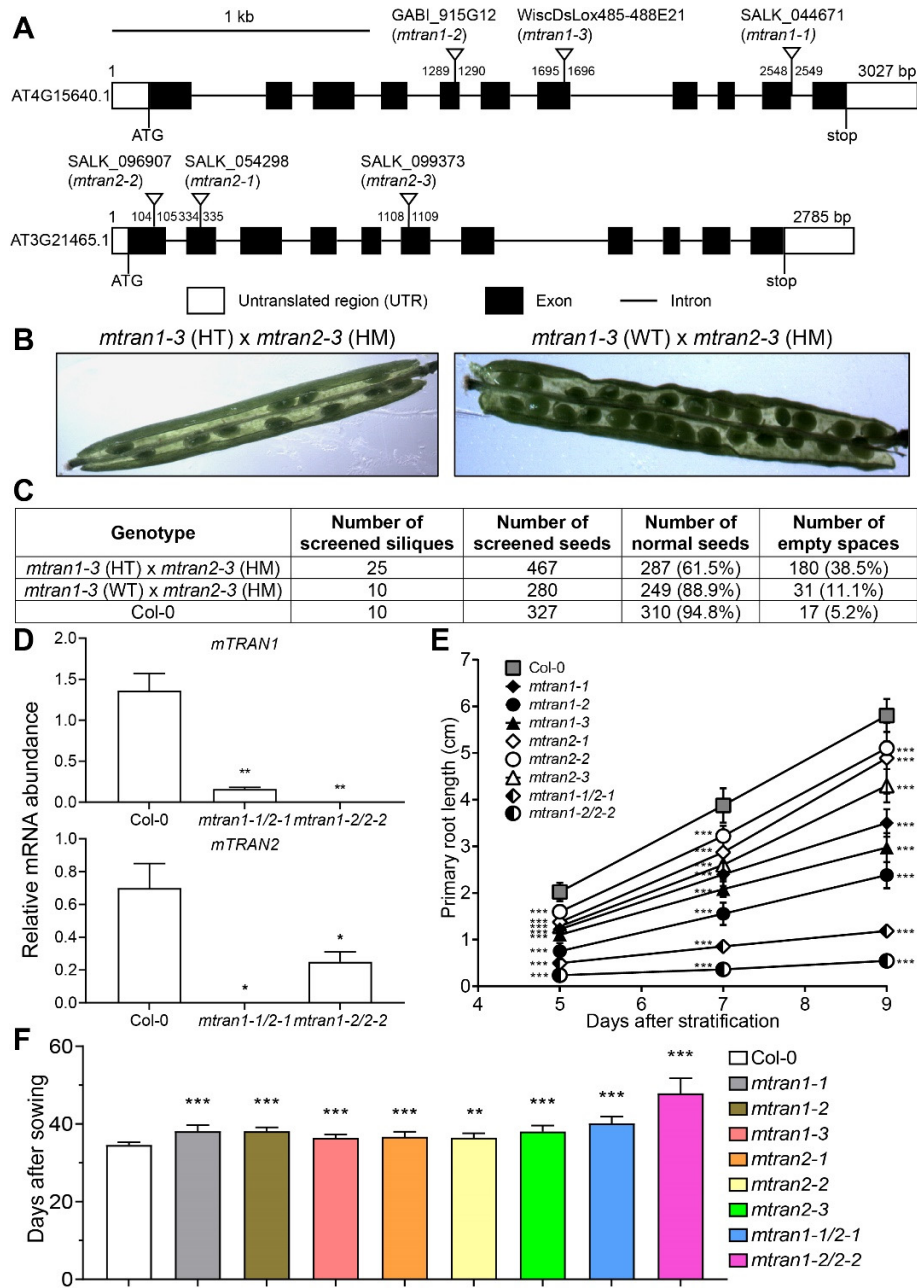
The sequences of genes analyzed in this article can be found in TAIR under the following accession numbers: *AT4G15640* (*mTRAN1*), *AT3G21465* (*mTRAN2*), *AT3G22370* (*AOX1a*), *AT2G21640* (*UPOX1*), *AT1G05680* (*UGT74E2*), *AT2G20800* (*NDB4*), *AT5G09570* (*AT12CYS-2*), *AT2G41730* (*HRG1*), *ATMG00270* (*NAD6*), *ATMG00510* (*NAD7*), *ATMG00070* (*NAD9*), *ATMG00220* (*COB*), *ATMG00160* (*COX2*), *ATMG01190* (*ATP1*), *ATMG00480* (*ATP8*), *ATMG01080* (*ATP9*), *ATMG00290* (*RPS4*), *ATMG01390* (*RRN18*), *ATMG00020* (*RRN26*) and *AT5G25760* (*UBC21*).



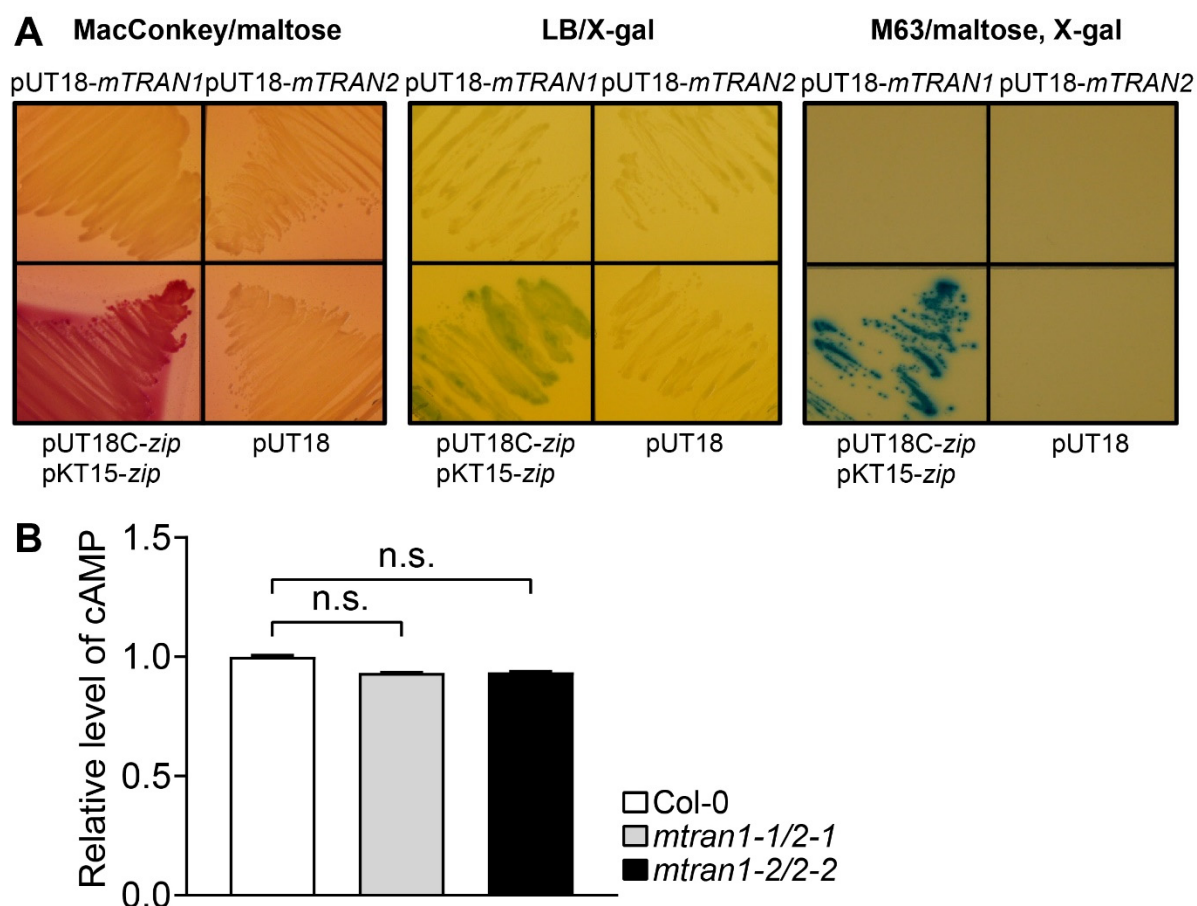
**Figure S1. Alignment of the conserved parts of mTRAN proteins from land plant species.** All proteins sequences were collected from PLAZA 4.5 (71). Multiple sequence alignment (MSA) was generated using the algorithm MUSCLE followed by MSA trimming within the PLAZA platform.



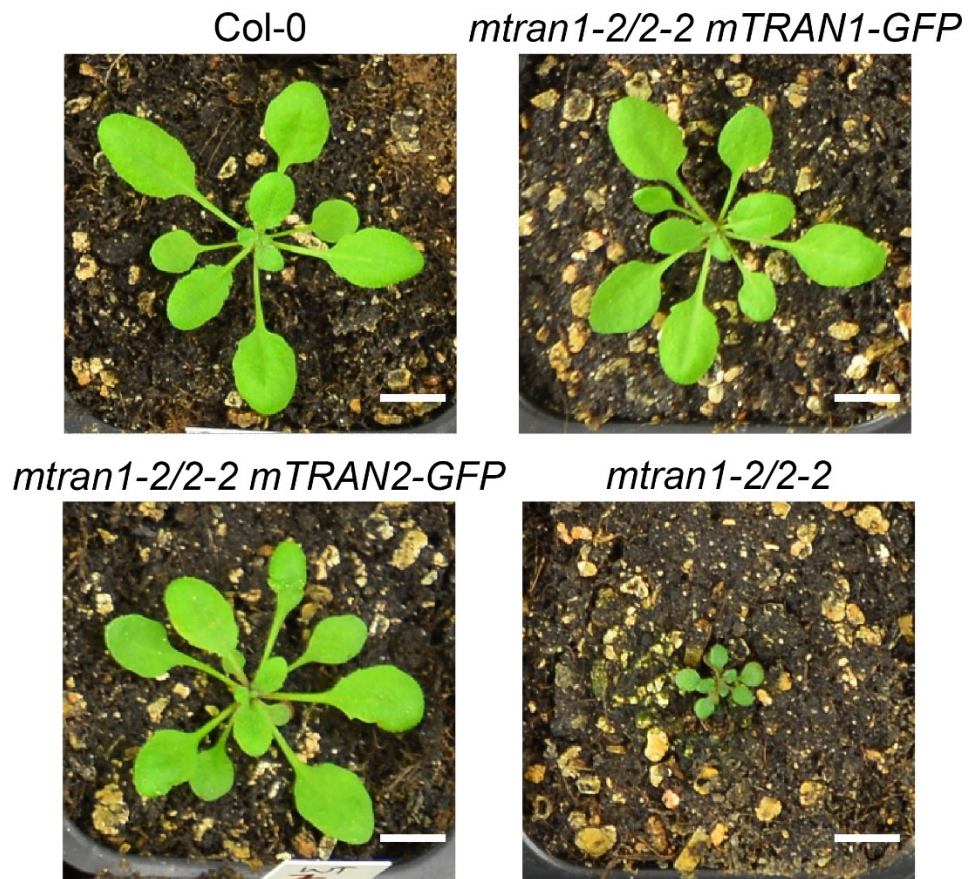
**Figure S2. Expression patterns of *mTRAN1* and *mTRAN2* in different tissues of *Arabidopsis thaliana*.** The Arabidopsis Genome Identifiers (AGI) of *mTRAN1* and *mTRAN2* were queried in Arabidopsis eFP Browser (<http://bar.utoronto.ca/efp/cgi-bin/efpWeb.cgi>) (99) using Data Source “Klepikova Atlas”.



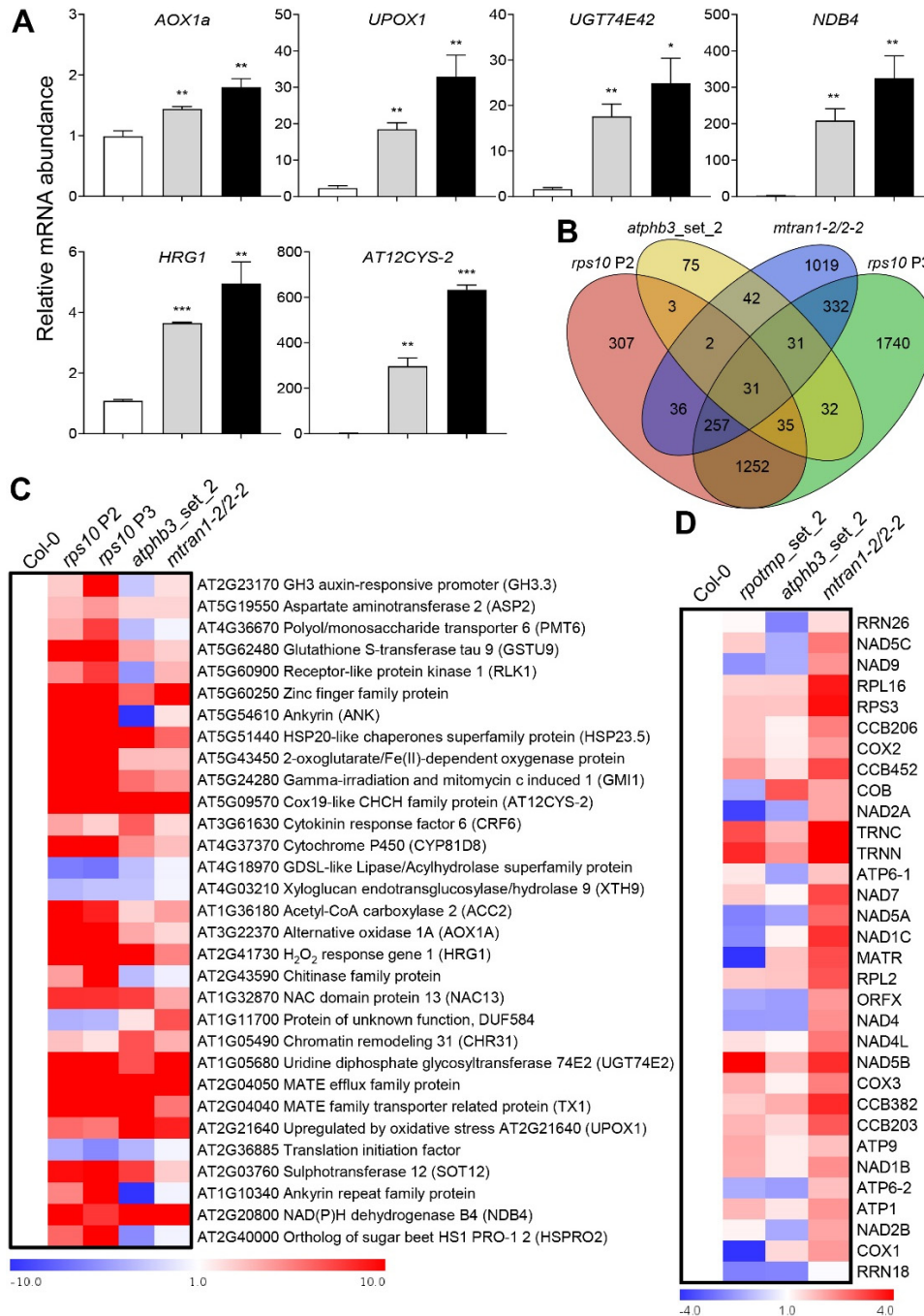
**Figure S3. Phenotypic analysis of the double knockout *mtran* mutants.** **A.** *mTRAN1* and *mTRAN2* T-DNA insertion positions. White boxes = untranslated regions (UTRs), black boxes = exons, black lines = introns. **B.** *mtran1-3/2-3* is embryo lethal. Pictures of dissected siliques of *mtran1-3* (heterozygous (HT)) x *mtran2-3* (homozygous (HM)) and *mtran1-3* (wildtype (WT)) x *mtran2-3* (HM) are shown. **C.** Number of seeds and empty space of dissected siliques of *mtran1-3* (HT) x *mtran2-3* (HM), *mtran1-3* (WT) x *mtran2-3* (HM) and Col-0 (the WT) was analyzed. **D.** The loss of function of *mTRAN1* and *mTRAN2* transcripts in *mtran1-1/2-1* and *mtran1-2/2-2*. Seedlings at developmental stage 1.04 (26) were collected in pools and relative mRNA abundance were measured by qRT-PCR (n=3) and normalized to Col-0 samples ( $\pm$ SE). **E.** Primary root length of vertically-grown plants (means  $\pm$  SD, n=15). **F.** Determination of flowering time of plants grown in soil (means  $\pm$  SD, n=9). Statistical significance was based on Student's *t* test with Bonferroni correction (\*= $P$ <0.05, \*\*= $P$ <0.01, \*\*\*= $P$ <0.001).



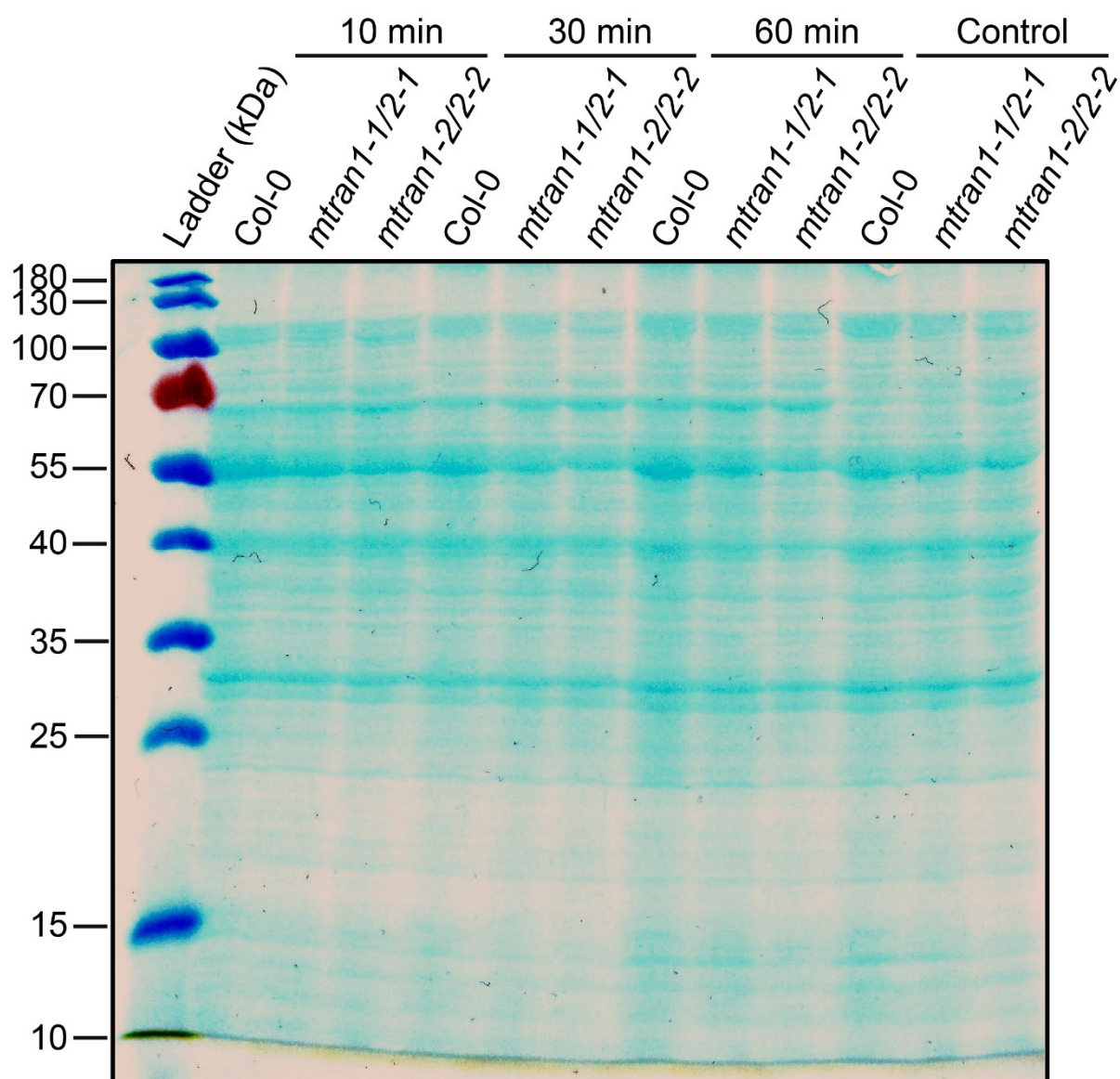
**Figure S4. mTRAN1 and mTRAN2 do not have adenylyl cyclase activity.** **A.** The bacterial cAMP synthase complementation assay was based on the Bacterial Adenylate Cyclase Two-Hybrid System. For positive control, pUT18C-*zip* and pKT15-*zip* were co-transformed into *BTH101*. For negative control, the empty vector pUT18 was transformed into *BTH101*. Transformed cells were plated on MacConkey/maltose (left panel), LB/X-gal (middle panel) and M63/maltose, X-gal media (right panel). **B.** cAMP content measurement *in planta*. The endogenous cAMP content of the *mtran* double mutants was normalized to Col-0. Statistical significance was based on Student's *t* test ( $n=3$ ) ( $\pm$ SE). n.s.=non-significant.



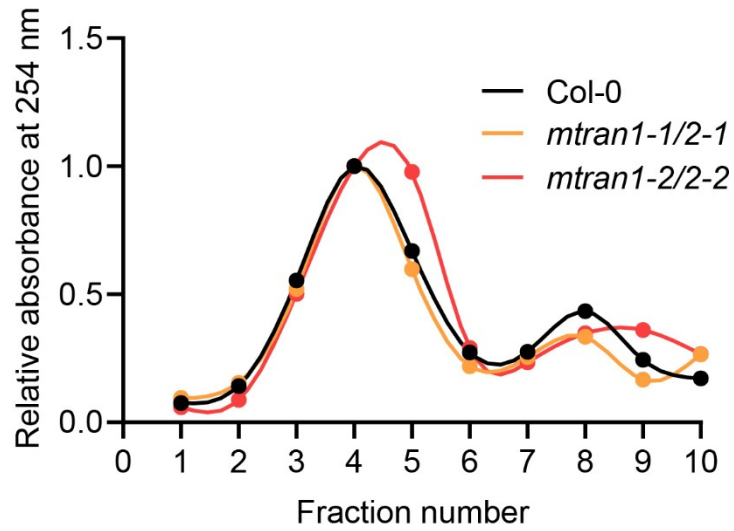
**Figure S5. Phenotypes of *mtran1-2/2-2 mTRAN1/2-GFP* complementation lines.** The picture of representative plants was taken on the 25<sup>th</sup> day of growth. Scale bar: 1 cm.





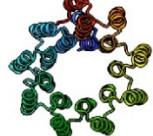






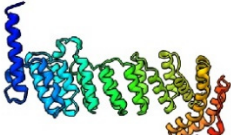
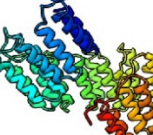
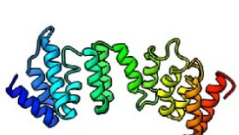




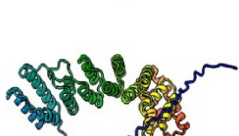




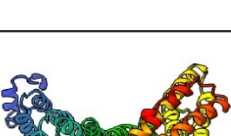
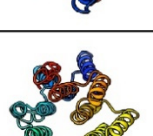








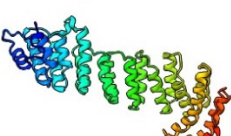
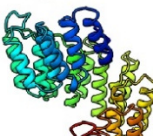







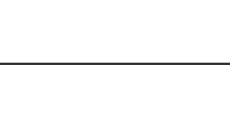
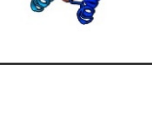
**Figure S6. Nuclear and organellar transcriptome comparison of the *mtran1-2/2-2* mutant with other Arabidopsis mutants defective in fundamental mitochondrial functions. A.** Loss of *mTRAN1* and *mTRAN2* results in upregulation of mitochondrial retrograde/unfolded protein response (UPR<sup>mt</sup>) signalling markers. Relative mRNA abundance of *mtran1-1/2-1* and *mtran1-2/2-2* were measured by qRT-PCR (n=3) and normalized to Col-0 ( $\pm$ SE). Statistical significance was based on Student's *t* test (\*= $P<0.05$ , \*\*= $P<0.01$ , \*\*\*= $P<0.001$ ). **B.** Venn diagram represents common DEGs among *mtran1-2/2-2*, *rps10* P2 and P3 and *atphb3*. **C.** Heat map of 31 common DEGs among *mtran1-2/2-2*, *rps10* P2 and P3 and *atphb3*. Color bar indicates linear fold change. **D.** Heat map of mitochondrially-encoded transcripts differentially expressed among *mtran1-2/2-2*, *rpotmp* and *atphb3*. Color bar indicates linear fold change.



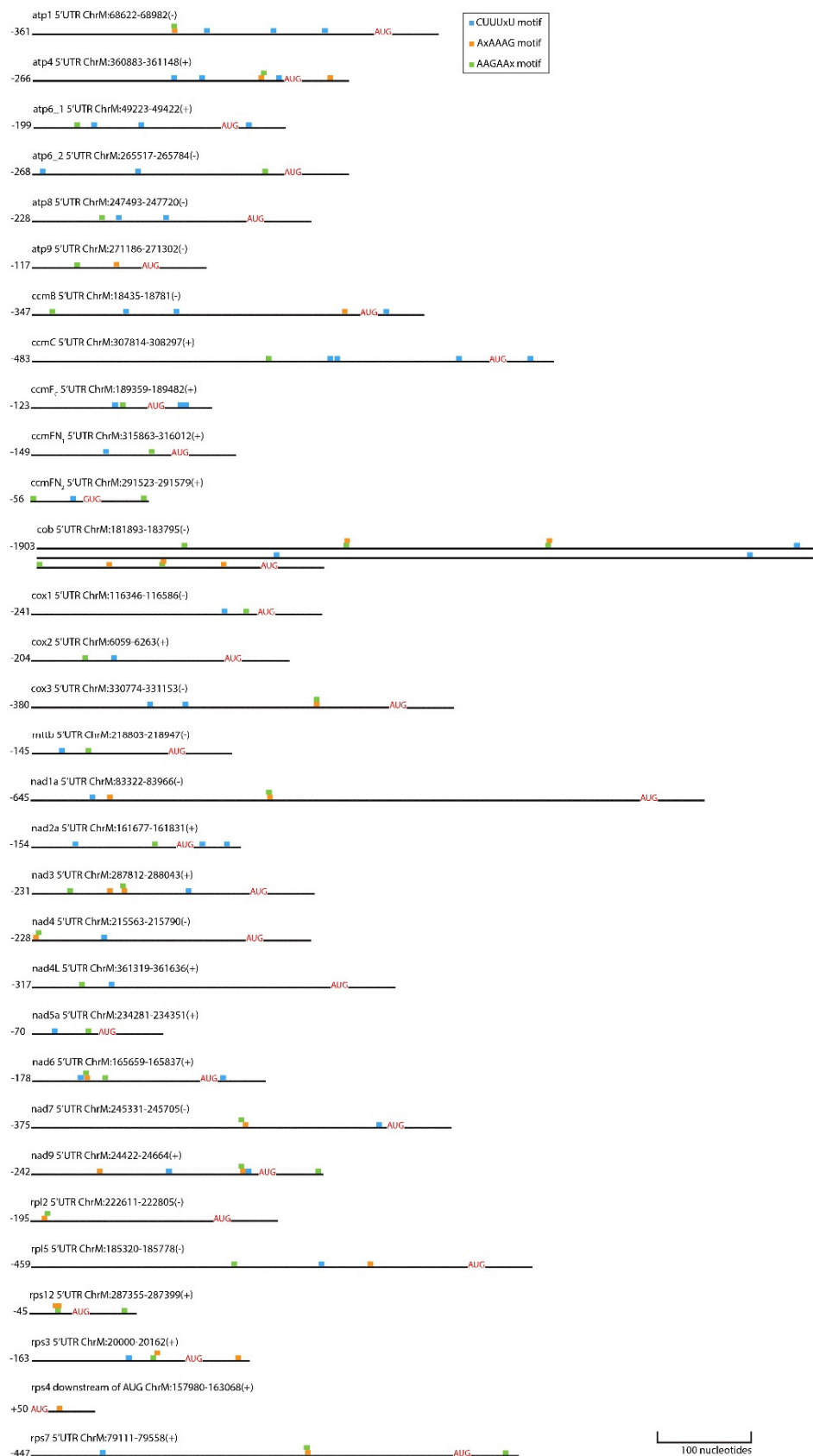
**Figure S7. Coomassie Brilliant Blue staining of mitochondrial proteins resolved on SDS-PAGE after in organello protein synthesis assays.** The assays were conducted for 10, 30 and 60 min using purified mitochondria from Col-0, *mtran1-1/2-1* and *mtran1-2/2-2*. In the control reactions (60 min), sodium acetate was used as substrate to assess bacterial contamination. The molecular weight (kDa) is shown on the left side of the gel.



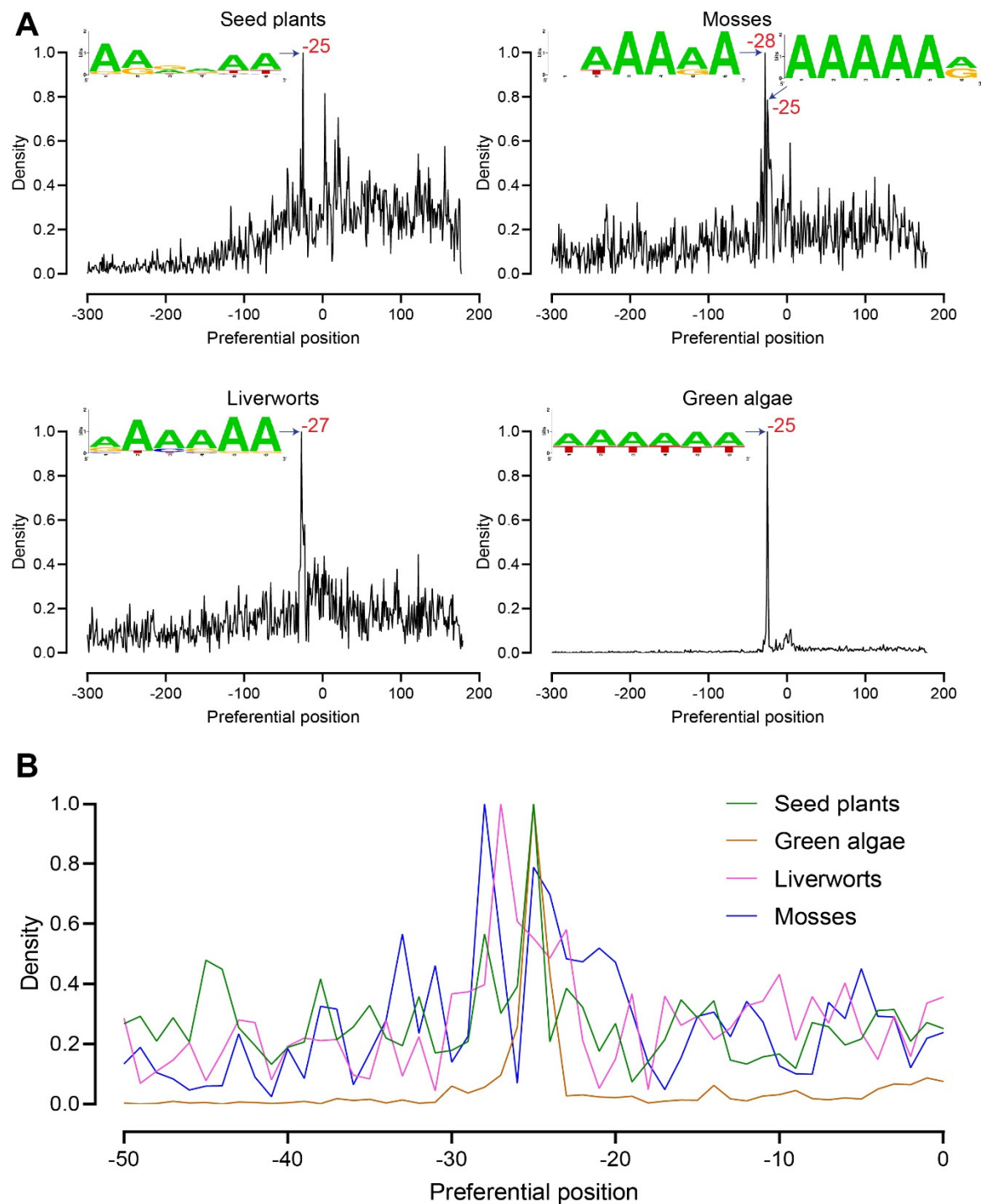
**Figure S8. Sucrose gradient absorbance profiles of polysome fractionation analysis.** The cell lysates obtained from WT and the *mtran* double mutants were loaded onto 15-55% sucrose gradients and fractionated by ultracentrifugation. After that, 10 fractions were collected from the top of the gradient, RNA was prepared and the absorbance of each fraction was measured at 254 nm to estimate ribosome distribution.

	AlphaFold	RoseTTAFold	iTASSER	Waltz et al. 2020
mTRAN1				
				
				
				
				
				
mTRAN2				
				
				
				
				
				

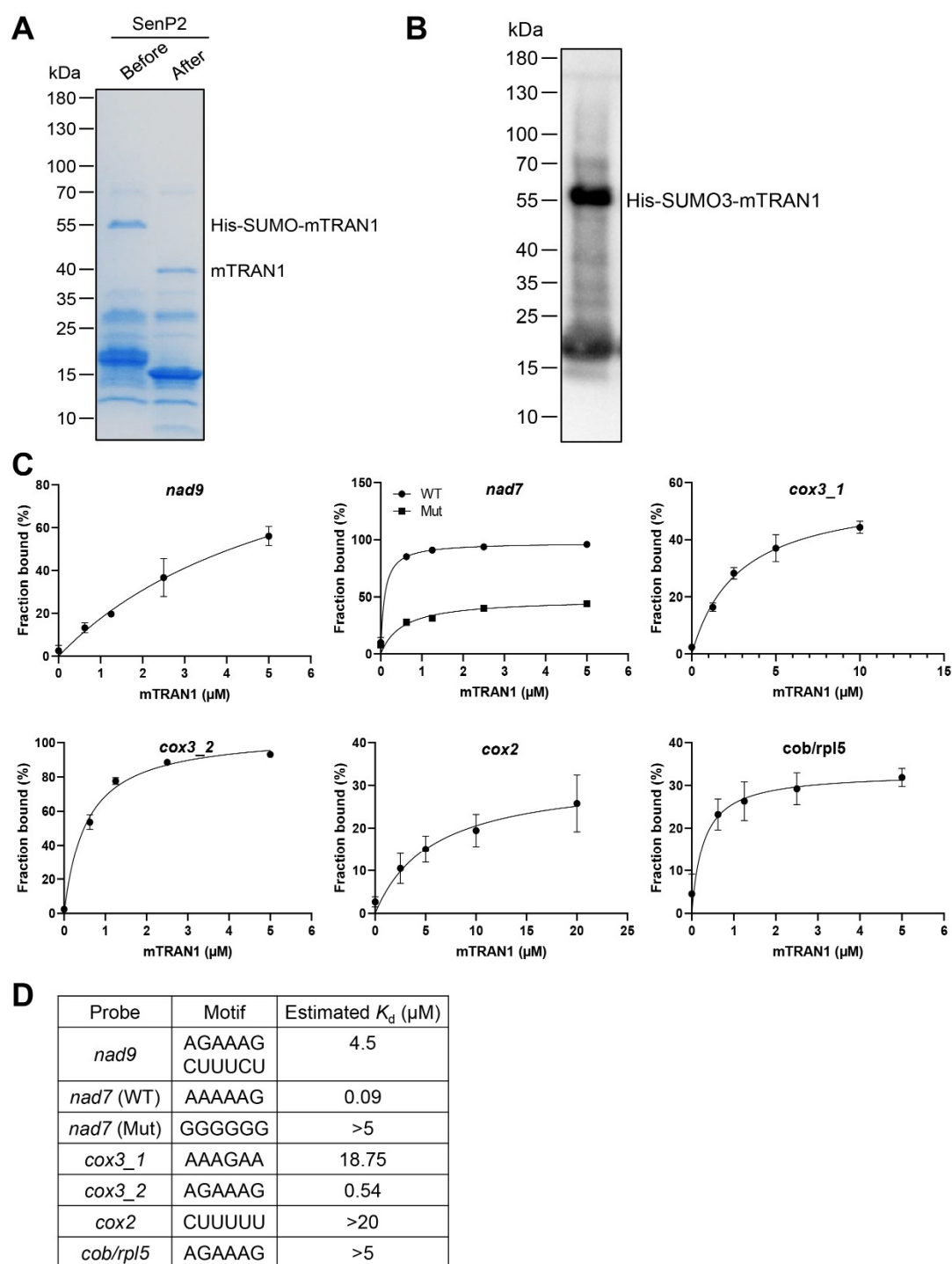
**Figure S9. Predicted protein structures suggest that mTRAN1 and mTRAN2 have PPR protein like-structures.** Protein structures of mTRAN1 and mTRAN2 without mitochondrial targeting sequences predicted by MitoFates (37) were modelled by AlphaFold (38), RoseTTAFold (39) and iTASSER (40). The predicted structure of mTRAN1 from Waltz et al (16) is also presented to be compared with their other predicted structures.



**Figure S10. The position of potential mitoribosome binding sites in the 5' UTRs and +50 nucleotides downstream of start codon of mitochondrial mRNAs.** Blue box = CUUUxU. Orange box = AxAAAG. Green box = AAGAAx. Scale bar = 100 nucleotides. AUG/GUG = start codon.



**Figure S11. Motif analysis of the 5' regions of mitochondrial protein coding genes in seed plants, mosses, liverworts and green algae. A.** The preferential positions and density of enriched hexameric sequence in the 5' genomic regions of mitochondrial protein coding genes as detected in seed plants, liverworts, mosses and green algae using “PLMdetect”. The sequence logos visualise the consensus sequence of the enriched sequences (PLMdetect score >5) weighted for in how many genes they occur. **B.** Close-up of the preferential positions between -24 and -29 containing the A/U-rich regions in the 5' regions of mitochondrial protein coding genes in seed plants, liverworts, mosses and green algae.



**Figure S12. mTRAN1 can directly bind potential mitoribosome binding sites.** **A.** His-SUMO3-mTRAN1 purified from *E. coli* was digested with the protease SenP2 to remove the tag His-SUMO3. The purified protein were resolved on SDS-PAGE followed by Coomassie Brilliant Blue (CBB) staining. **B.** Western blot using an antibody against the 6xHis tag confirmed the purification of His-SUMO3-mTRAN1 from *E. coli*. **C.** Fraction bound (complex) and free RNA probes from REMSAs performed with mTRAN1 protein amounts up to 20  $\mu$ M were quantified and used for plotting (n=3). **D.** The  $K_d$  of mTRAN1 protein ( $\mu$ M) for each probe was estimated (n=3).

## Supplementary Data (separate files)

### Data S1. Mitochondrial proteomic study of the *mtran* double mutants.

**Data S2. Proteins identified as interacting with mTRAN1 and mTRAN2 in planta.** **A.** A summary list of proteins co-immunoprecipitated with mTRAN1-GFP and mTRAN2-GFP. **B.** All proteins identified as interacting with mitoGFP in planta. **C.** All proteins identified as interacting with mTRAN1 and mTRAN2 in planta.

### Data S3. RNA-seq analysis of *mtran1-2/2-2*.

### Data S4. Gene ontology analysis of DEGs found in RNA-seq analysis of *mtran1-2/2-2*.

**Data S5. Microarray and RNA-seq datasets used for meta-analysis.** **A.** List of DEGs of *mtran1-2/2-2* versus other mitochondrial perturbations in Arabidopsis. **B.** Comparison of common pairwise DEGs calculated via the Sørensen-Dice similarity coefficient.

**Data S6. Organellar transcriptome analysis of *mtran1-2/2-2*.** **A.** Mitochondrial transcriptome of *mtran1-2/2-2*. **B.** Chloroplastic transcriptome of *mtran1-2/2-2*. **C.** Mitochondrial transcriptome of *mtran1-2/2-2* versus *rpotmp* versus *atphb3*.

### Data S7. Editing (A) and splicing (B) analysis of mitochondrial transcripts of *mtran1-2/2-2*.

**Data S8. Motif analysis of the 5' UTRs of mitochondrial mRNAs of *Arabidopsis thaliana* using MEME.** **A.** The 5' UTR sequences of mitochondrial mRNAs. **B.** Motif analysis of the mitochondrial mRNA's 5' UTRs without putative inter-cistronic 5' UTRs using MEME search tool and manual search. **C.** Motif analysis of the mitochondrial mRNA's 5' UTRs with putative inter-cistronic 5' UTRs using MEME search tool and manual search.

**Data S9. Motif analysis of the 5' regions of mitochondrial mRNAs of seed plants (A), liverworts (B), mosses (C) and green algae (D) using PLMdetect.**

**Data S10. Motif analysis DiffSegR RIP-seq.** **(A)** Sequences of overrepresentation of mTRAN1-specific immunoprecipitated RNA fragments vs. the GFP-control background calculated by DiffSegR (Padj<0.05). **(B)** MEME motif search results.

### Data S11. Analysis of mitochondrial ribosome footprints of the *mtran* double mutants.

**Data S12. *mTRAN* mRNA half-life and abundance vs other PPR proteins (0-1 intron).** **A.** *mTRAN* mRNA half-life vs other PPR proteins (0-1 intron). **B.** *mTRAN* mRNA abundance vs other PPR proteins (0-1 intron).

### Data S13. All oligonucleotides used in this study.